

Design of a valveless organ-on-chip micropump

A new take on on-chip actuation
for organ-on-chip devices

Suzanne
Onderdelinden



Design of a valveless organ-on-chip micropump

A new take on on-chip actuation
for organ-on-chip devices

by

Suzanne
Onderdelinden

to obtain the degree of Master of Science
at the Delft University of Technology,
to be defended publicly on June 26th 2020

Student number: 4016920
Project duration: March 1, 2019 - June 26, 2020
Thesis committee: Prof. P.M. Sarro, TU Delft (chair)
Dr. M. Mastrangeli, TU Delft (supervisor)
Dr. M.K. Ghatkesar, TU Delft

An electronic version of this thesis is available at <http://repository.tudelft.nl/>.

Cover image: plastinated blood vessels of the heart

Retrieved from: <https://www.thecardiologyadvisor.com/home/conference-highlights/aha-2018-meeting-highlights/>

[canakinumab-may-reduce-cv-events-in-patients-post-mi-with-residual-inflammatory-risk/](https://www.thecardiologyadvisor.com/home/conference-highlights/aha-2018-meeting-highlights/canakinumab-may-reduce-cv-events-in-patients-post-mi-with-residual-inflammatory-risk/)

Preface

During a worldwide pandemic, several months later than intended, being an elected official and upcoming teacher and based on experimental modelling rather than physical experiments: neither of those were circumstances I had anticipated during my graduation when I started this thesis in March 2019. It has been quite a ride! And although there is much to still be achieved in this interesting subject, it is time to pass on the torch.

There are many people who have played their part in bringing this to a good ending. First of all I should thank Massimo and Paul for their patience and hard work to help me get where I am now - and everyone else at ECTM who helped me and who are too many to count. My parents, without whom I wouldn't be here in multiple ways; Chuqian, Mauricio, Raghutham and Caitlin for more or less intellectual conversation in LB1,490, board games and dank memes; Hande, for good times with heavy metal and cats; Mirte, my RPG siblings Jisk, Gio, Yanick, Gudrun and Chris for social distance socializing - particularly Gio for excellent Matlab googling skills, and all the others I'm forgetting: you're awesome. And obviously, enormous thanks to Samir, who believed in me when I didn't and without whom this whole thing would have been far less enjoyable, to say the least. All of you, thanks, and I'll see you at my graduation party - whenever that may be.

Delft, June 12th, 2020

Abstract

In the last few years organ-on-chip (OoC) has been emerging as a new method for more reliable research to screen the effects of new drugs on the body. This is a novel technology mimicking the *in vivo* environment of tissue cells, making it a more suitable candidate for experimentation than traditional 2D cell cultures. However, in order to ensure smooth and swift implementation of this technique, some issues must be addressed first. One of these issues concerns perfusion: most OoC devices require external equipment to provide the necessary dynamic flow that makes the OoC unique, so that cells experience continuous fluid shear and are perfused sufficiently.

In this thesis a model of an on-chip electro-polymeric pump is designed for application on an OoC. From a background study the design aims are defined: a membrane actuated pump with a nozzle-diffuser channel providing pump action. The membrane is made from ionic polymer-metal composite (IPMC), a material that deforms under electric current which is produced at TU Delft with the intention to use it in OoC applications. Its low voltage operating range and its biocompatibility make it an excellent candidate for this. Furthermore, the nozzle-diffuser elements avoid the need for moving elements inside the channel, instead providing pump action based on a pressure gradient over the nozzle elements. Finally, three design aims are defined, being: high flowrate, high flow pulse and low flow rate and pulse applications, corresponding to various needs in the OoC field.

A base model is designed using COMSOL Multiphysics [1] software, using similar devices described in literature. The model consists of a combination of solid mechanics (for membrane movement), fluid mechanics (for flow movement) and a fluid-structure interaction module to combine the two. This model is then tested for a range of parameters, first independently and later in pairs. General conclusions drawn from these simulations include:

- Between the membrane displacement and -frequency (which can both be varied after fabrication), the membrane displacement magnitude affects the output more significantly than actuation frequency
- The membrane width is positively correlated with flow rate output and pulse amplitude
- The channel depth is positively correlated with flow rate output, but only if the membrane displacement scales along with it
- A long slender nozzle yields lower flow output than a short, squat nozzle
- The results from this model are consistent with nozzle-diffuser theory, stating that nozzle resistance and membrane movement affect the flow most significantly.

This leads to three designs according to the three application wishes expressed earlier.

The pump is designed such that it can be manufactured on a silicon wafer using electronics cleanroom equipment. The combination with the process developed for IPMC provides a novel pumping mechanism that has the potential to fully integrate an important aspect of an OoC on-chip, greatly increasing user friendliness and allowing for wider implementation of this technology.

Contents

Preface	iii
Abstract	v
Introduction	1
1 Background	3
1.1 Thesis relevance and purpose	3
1.2 Biomedical fundamentals	4
1.2.1 Organ physiology basics	4
1.2.2 Medical drug development	5
1.3 Organ-on-chip technology	6
1.3.1 Organ-on-chip fundamentals	6
1.3.2 Exemplary OoC successes	7
1.4 Fluid behaviour and manipulation	9
1.4.1 Fluid mechanics and microfluidics	9
1.4.2 Pumping mechanisms	10
1.4.3 The nozzle-diffuser approach	12
1.4.4 Flow rate in biological applications	13
1.5 Microfabrication	14
1.5.1 Materials for biological on-chip applications	14
1.5.2 MEMS technology	14
1.6 Conclusion	15
2 Pump modelling	17
2.1 Design outline and justification	17
2.2 Physics of the model	18
2.2.1 Solid Mechanics	18
2.2.2 Creeping Flow	18
2.2.3 Global ODEs and DAEs	18
2.2.4 Multiphysics	19
2.3 Parameter identification	19
2.3.1 Operational parameters	19
2.3.2 Chamber parameters	20
2.3.3 Nozzle-diffuser parameters	20
2.4 Modelling work flow	20
2.5 Initial design: literature background	21
2.6 Discussion and iteration	22
2.7 Conclusion	22
3 Simulations	23
3.1 Model verification	23
3.1.1 Eigenvalue analysis	23
3.1.2 Laminar flow	24
3.2 Model evaluation and characterization process	27
3.2.1 Base model evaluation	27
3.2.2 Initial characterizations (process)	28
3.2.3 Interaction characterizations (process)	28
3.2.4 Alternative configuration	29

3.3	Initial characterization (results)	29
3.3.1	Sample time	29
3.3.2	Frequency	30
3.3.3	Displacement	31
3.3.4	Membrane width.	31
3.3.5	Channel depth	32
3.3.6	Nozzle angle	34
3.3.7	Nozzle width	34
3.3.8	Nozzle length	35
3.4	Intermediate conclusions	35
3.5	Interaction characterization (results)	36
3.5.1	Membrane frequency-displacement correlation	36
3.5.2	Channel depth-membrane width correlation	36
3.5.3	Nozzle parameter correlation	37
3.5.4	Nozzle width-membrane displacement correlation	39
3.6	Alternative configuration results	40
3.7	Conclusion	40
4	Results	41
4.1	Design overview	41
4.2	High flow rate design	41
4.3	High pulsing design	43
4.4	Low flow rate and pulsing design	44
4.5	Conclusion	46
5	Recommendations	47
5.1	Modelling and simulation improvements	47
5.2	Fabrication	48
5.3	Testing	48
5.4	Conclusion	49
6	Conclusion	51
	Bibliography	53
	Appendices	59
A	Beam theory	59
B	Supplementary plots	61
B.1	Frequency sweep	61
B.2	Channel depth sweep	62
B.3	Nozzle parameter sweeps	62
B.4	High flow rate design	63
C	Matlab scripts	65
C.1	Sample time analysis	65
C.2	Single parameter sweep analysis	66
C.3	Flowrate calculation	67
D	Model sketches	69
	Acronyms	71
	Glossary	73

Introduction

During the completion of this master thesis, the world is facing an unprecedented health crisis. People work from home, events are cancelled, the economy has grinded to a halt. Meanwhile, policy makers dealing with appropriate measures to keep the COVID-19 pandemic at bay have only one question in mind: when will there be a vaccine? It is once more clear that to battle increasingly complex health care matters, quick and reliable testing methods are needed to develop medication.

Organ-on-chip (OoC) technology is an application of microfluidic technology that is expected to change the way drugs are developed and human physiology is studied. These tiny models of human organs (and possibly other systems) rely on complex on-chip systems to function. One of these essential systems is the perfusion, for which a pumping mechanism is required. While this can relatively easily be done using an externally attached pump, an on-chip solution is likely to improve user-friendliness, experiment setup times and handleability, and thus facilitating implementation of this improved means of analyzing interaction with the human body. For this reason, this thesis aims to design an on-chip pumping device suited for microfluidic OoC applications

In the background of this thesis, first a more extensive problem statement is given and background is provided on organ physiology, organ-on-chip devices, fluid mechanics and electronics materials and fabrication. This leads to a design proposal: a pumping device with pump action generated by nozzle-diffuser elements and an actuating membrane. The membrane material will be ionic polymer-metal composite (IPMC): a biocompatible material exhibiting deformation behavior under low electric current, which makes it an excellent candidate for OoC applications. Three optimal results will be sought: for high flow rate, high flow pulsing and for low flow rate and pulsing (**chapter 1**). With this knowledge and context in mind, a COMSOL Multiphysics [1] model is built using a combination of solid mechanics (for the moving membrane) and laminar flow fluid mechanics (for the fluid flow), coupled through the multiphysics module. Using literary references the initial setup is made, which serves as the base model for further parameter sweeps to look for the design optima (**chapter 2**). The simulations are laid out in the next chapter, by first defining the base model and then proceeding with parameter sweeps of model parameters and certain interaction studies. These tests and simulations lead to the three designs described earlier. Furthermore, an additional study is performed to an alternative configuration with a multi-nozzle model (**chapter 3**). These models are explained and studied in more detail in the next chapter, analyzing their behaviour and expected optimal performance conditions (**chapter 4**). Recommendations for continuation of this project have been listed for modelling and simulation, for fabrication and for testing of the device (**chapter 5**). The thesis is summarized and reflected upon in the conclusion (**chapter 6**).

In addition to this content, at the end of this thesis report a number of appendices can be found. These include a section on beam theory used to analyze IPMC movement (A), additional data plots of interest for the simulation results (B), MATLAB code used for data postprocessing (C) and additional sketches for the fabrication proposal (D). Note that no actual datasets are included: the postprocessed results are assumed most relevant: anyone interested can obtain the results themselves using the model which can be obtained from the author.

Readers of a digital version of this thesis report should note that all references to sections, figures, citations etc. are hyperlinked for easy navigation through the document. Additionally, many specific terms and all relevant abbreviations are listed in the glossary at the end of the report and these are hyperlinked in-text as well.

Background

This chapter provides the necessary literary background of relevant organ-on-chip (OoC) related fields for the rest of the thesis. It is different from the literature study conducted originally as the design has changed significantly requiring additional resources.

First and foremost some background is given on the thesis purpose and relevance: to develop an on-chip pumping device to accommodate larger scale applications of OoC devices (section 1.1). Firstly the biomedical context of the problem is sketched: its applications in drug development and the necessary background of organ physiology is given (section 1.2). This is put in the context of the eventual application, namely organ-on-chip. The fundamentals are given as well as some exemplary successful applications (section 1.3). For working with living material, nutrients are required through a microfluidic system: general fluid mechanics, microfluidics are treated along with nozzle-diffuser theory necessary for the chosen design (section 1.4). As the design shall be produced using micro-electronical mechanical systems (MEMS) technology some materials and fabrication techniques are introduced, including the IPMC material (section 1.5). In the conclusion a brief summary is given (section 1.6).

1.1. Thesis relevance and purpose

Costs of newly developed drugs are at an all-time high: partly due to increased regulations but also due to the large number of new drugs (investigational new drug (IND)) that are retracted due to unforeseen adverse effects. There is a great need for inexpensive early-phase testing methods that can reliably predict the behaviour of INDs as soon as possible. This can prevent retraction later on, avoiding (permanent) damage in test volunteers and patients and saving resources on INDs that will not make it to the finish line. (More on this is treated in 1.2.2.)

A promising solution for this is the organ-on-chip (OoC) device: a microfluidic device that mimics the physiology of an *in vivo* organ. (More on this is treated in section 1.3.) Although this has the potential to become an excellent human model, there are some things that prevent its swift implementation. Most current OoCs are actuated pneumatically, using an external device to provide sufficient shear stress in the channels, as well as cell medium for nutrients. However, these external devices are inconvenient in use in such small devices and introduce more room for human error. An on-chip pumping device would solve multiple problems at once: it reduces errors, both in use and fabrication, and allows for a more reproducible device. These solutions will make the OoC a more interesting option for widespread implementation in conventional lab settings. The device might also be implemented in the TU Delft Cytostretch platform, now requiring an external pumping device [12].

The aim of this thesis is to design and model an on-chip pumping device to be applied in an OoC. This is done using the developments at the ECTM group of TU Delft[23] on the use of ionic polymer-metal composite (IPMC), a biocompatible material that deforms under electric current and which is known to work well in a fluidic environment. The device is modelled in COMSOL Multiphysics [1] and fabrication and testing recommendations are given for (a) future project(s).

The questions answered in this chapter are what the physiological requirements are of the pump and the

best configuration of the pumping mechanism is chosen. Furthermore, background information is given concerning previous OoC projects of interest and material options are discussed.

1.2. Biomedical fundamentals

The OoC is a biomedical device with promising opportunities for the drug development field in particular. First some of the basic required knowledge of organ physiology is given in the context of requirements of OoC models of such organs (1.2.1). Following, the need for innovation in drug development is illustrated by explaining the traditional process and some critical points where this currently fails (1.2.2). With this in mind, the following section concerns more concrete OoC technology aspects.

1.2.1. Organ physiology basics

When creating human models to mimic the *in vivo* environment, some crucial aspects must be taken into account. Cell physiology but also the mechanical environment are directly affected by the device fluid dynamics. Below, some properties and factors of interest are listed for selected organs and pathologies (table 1.1). Note that this table keeps the application of a drug testing device in mind and normal organ function is considered. As these details are not always specified in articles on OoC devices, the properties and factors of interest are primarily based on anatomy and physiology theory [19] or other literature when appropriate. Note also that terminology is hyperlinked and listed in the glossary.

	Area of interest	Physiology of interest	(Fluid) mechanics involved
Intestine	Absorption of most ingested components and nutrients into the blood	Formation of microvilli for nutrient absorption, sustaining of the microbiome [14]	Fluid shear flow on the microvilli side of the membrane [28]
Liver	Metabolization or secretion of certain components in blood[19]	Metabolism through hepatic lobules or hepatocytes	High blood volume throughput, toxicity sensitivity [27]
Heart	Contraction of cardiac muscular tissue	Cardiac muscle cells and cardiac potential [21]	Strong blood flow, possibly adjustable
Lung	Gas exchange over the alveolar membrane	A thin surfactant-coated membrane of around 0.5 μm [11]	Surfactant for surface tension on the gas side of the membrane, very low fluid pressure (1-2kPa)
Blood-brain barrier (BBB)	Permeability (or impermeability) for certain compounds	A threefold membrane around which the astrocytes fold [37]	High wall shear stress (0.3 to 2 Pa)
Kidney	Filtering and excretion of certain substances and wastes	Blood filtering mechanisms (nephrons and collecting ducts) [15]	High blood volume throughput
Vasculature	Growth and healing mechanisms (angiogenesis description)	Cell differentiation behaviour under several conditions	Pulsating flow (depending on the location)
Tumor	Development and growth, as well as personalized medicine	Varying, high nutrient demand	Varying. high blood supply
Atherosclerosis	Development, growth and rupture	Endothelial damage, lipid accumulation and fibrous cap formation	Stiffened (calcified) walls and accompanying increased pressure

Table 1.1: An overview of organ and pathology functions and mechanics, based on conclusions drawn from anatomy and physiology [19]

The small intestine is important in drug development: many drugs are administered orally and need to pass it safely to reach the bloodstream at all. This is known as the first-pass effect: if the drug is metabolized by the body before entering circulation its availability is more limited [13]. Physiologically relevant conditions

essential to take into account are peristaltic motion and dynamic flow, which triggers the formation of three-dimensional microvilli, mucus and tight junctions [28]. These are essential structures forming the barrier to the bloodstream. In conventional models without dynamic flow these did not form [13].

The intestine relates close to operation of the liver, which is why they are often paired when modelling first-pass drug metabolism. It is even suggested that isolated liver models barely reflect real life: interaction between them is crucial in drug metabolism [5][38]. In a review by Olson et al. it was shown that hepatic toxicity was listed as reason for withdrawal in more than half of retracted studied drugs (while these toxicities were not seen during animal experimentation) [27]. This suggests that the liver is quite sensitive to medication (and that these are poorly predicted by animal experimentation).

A different area of interest is the heart and medication for treating cardiovascular disease. It appears many cardiac pathologies are hereditary or a result of genetic disorder and take many years to develop, many times the lifespan of an experimental animal [29]. Similarly, atherosclerosis is a pathology rarely seen in animals, and conventional models lack the complex comorbidities involved in the development of this condition [2]. The same holds for cancerous tumors: they take long to develop and involve several comorbidities.

Another membrane-based organ is the lung, where fast exchange of gases is necessary. Another is the blood-brain barrier: a highly selectively permeable membrane only allowing certain compounds into the neural fluids. What such membranes have in common is that in order for the tissues to form properly sufficient flow shear is necessary [11][37]. This is a condition that can't be replicated in conventional 2D cell cultures or Transwells (an membrane insert to be placed in conventional lab wells for cell culturing).

Finally, a complex organ that is nonetheless a crucial factor in medication studies is the kidney. Even though its exact operation is still under research, models have been made for separate structures, such as the proximal tubule [15]. Its operation is crucial for drug effectivity, as the kidney will filter out active compounds and nephrotoxic substances might accumulate here [15].

1.2.2. Medical drug development

Pharmaceutical research for drug development consists of the steps below [36]

- Discovery: a so-called new chemical entity (NCE) shows positive results on a biological target.
- Lead optimization: the NCE physiological properties are assessed, including chemical composition, solubility and administering options (aerosol, capsule, intravenous etc.)
- Preclinical trials: *in vitro* testing is performed on isolated cells and animals to study effectivity, toxicity and metabolism effects.

If the NCE has passed these trials it is submitted as investigational new drug (IND) and proceeds to clinical trials after approval.

- Clinical phase I: administration of small amounts of the IND to healthy volunteers to determine dosing safety.
- Clinical phase II: the IND is applied to a small group of affected patients to determine effectivity on the treated pathology.
- Clinical phase III: large groups of patients are treated, including double-blind studies
- Submission to market: the IND obtains market approval and continues monitoring in post-approval trials for unforeseen (long term) side-effects.

This is an extensive process involving lots of research hours: from discovery to market submission takes 13.5 years on average [8]. The costs per compound rise significantly when an IND enters clinical trials, whereas many NCEs don't even make it past the optimization phase (figure 1.1)

It is in the interest of everyone that retraction of unsuccessful NCEs and INDs happens as early as possible, so that no valuable resources (research funds but also man hours, facilities and materials etc.) are wasted on eventually ineffective compounds.

Three reasons can be identified for this high rate of retraction [8].

1. Development processes involving *in vitro* models and animals are not optimized to predict efficiency and toxicity in humans. For animal experimentation it has been shown that tests often can't be replicated due to varying lab conditions, large discrepancies between human diseases and animal model diseases, and irregularities between different animals or animal strains [2].
2. Although safety concerns are well justified when it comes to (experimental) medication, consequently requirements that have to be met will sooner intensify than halt (or even lessen).

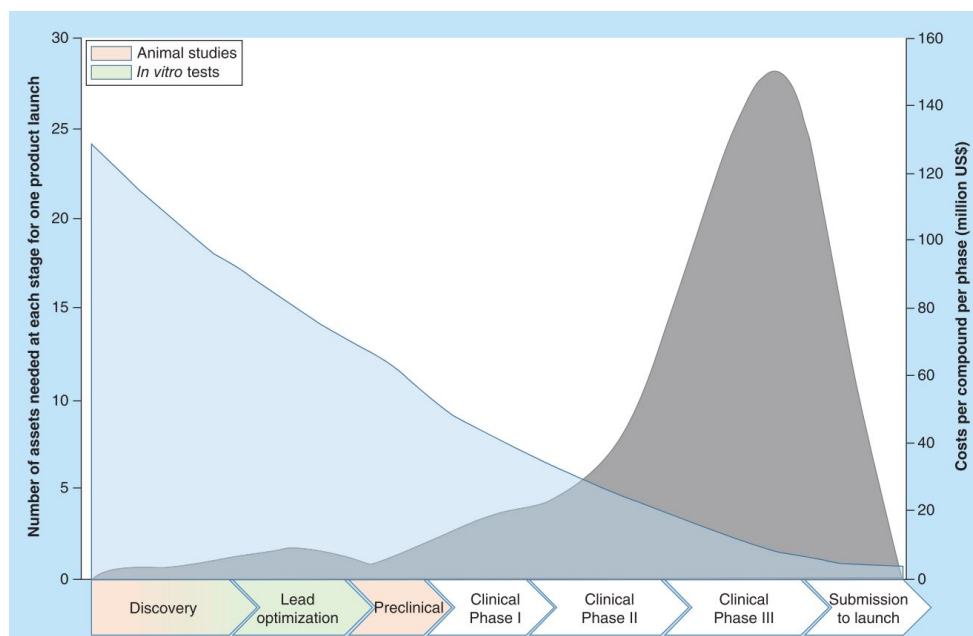


Figure 1.1: Assets and costs related to drug development. The left hand side depicts the average number of compounds needed for one successful market submission, and indicates in which phase the most NCEs and INDs are retracted. The right axis indicates the average costs per compound, which reaches its peak at phase III testing (involving large numbers of patients). It is in the interest of drug developers that unsuccessful compounds are identified as soon as possible to avoid expensive retraction later on. [8]

- Finally, current research and the diseases to be cured have become increasingly complex, leading to an increase in the amount of substances waiting to enter development [8].

In order for efficient application of resources a tool is needed that can assess drug efficiency and toxicity early on. A solution that was first founded by Huh et al (2007) [11] is called organ-on-chip (OoC), a microfluidic system which is physiologically similar to a human organ, and can therefore serve as a better model than traditional ones. With such instruments, future drug development can become more effective, less costly and avoid sacrificing vast numbers of animals.

1.3. Organ-on-chip technology

With the necessary background it is time to dive into the world of organ-on-chip (OoC). Firstly a deeper explanation is given as to what an OoC is and how it differs from related techniques (1.3.1). To illustrate this, some interesting OoC-devices from published literature are discussed (1.3.2).

1.3.1. Organ-on-chip fundamentals

As mentioned in 1.2.2, conventional drug development methods simply no longer suffice for the complexity, amount of work an required quality medicine faces. A solution was proposed in 2007 by Huh et al. who constructed a microfluidic system with the same functions as the capillary alveoli interface of a human lung [11]. This was developed to study the injury of airway epithelial cells as a symptom of pulmonary disease. This was not yet known as an OoC but it did have all the characteristics: a microfluidic device which displays the same mechanics and response as an organ (although on a smaller scale). These devices are used for experimental purposes such as drug development, as mentioned before, but there are more (future) possibilities: developmental study, the understanding of cell or even personalized medicine. As such devices are expected to provide more reproducible study results, it is not unthinkable that in the future they will omit the need for animal experimentation.

An OoC device differs from more basic techniques such as 2D cell cultures in several ways, such as the biophysical forces acting on a tissue. This is quite obvious in cardiac tissue but it also manifests itself in more subtle ways. An example is the blood-brain barrier BBB: the application of fluid shear is essential for the formation of the semipermeable membrane. This is seen when cell-cultures are compared to a BBB-on-chip: there are tighter junctions and a less permeable membrane (which is characteristic for the BBB) [31]. The intestine and the lung also rely greatly on fluid forces acting on it.

This is covered for when performing animal experimentation. These methods provide insight in the behaviour of NCEs and INDs in a complex metabolism, however, evidence suggests that they often fail to live up to the standards of scientific research [27][31]. For example: laboratory environment and standard routines in animal experimentation can affect study outcomes [2]. This affects the study at hand but affects reproducibility greatly as well. Furthermore, many diseases currently being cured are far more complex than the relatively simple issues that have been in the past [27]. Headaches, minor burn wounds and heartburn are ailments that (if not chronic) can be easily treated with well-tested products and found to work in almost all people. These are simple in relation to challenges currently being tackled such as rare forms of cancer, stroke and diabetes. The problem with them is that they, firstly, don't generally occur in animals[2]; secondly, they are often the consequence of underlying conditions that are difficult to introduce as comorbidity. Many researchers seem to be stuck in this loop, where valuable resources are spent on trying to make tiny humans out of mice, rather than to find real solutions - such as human models. Finally, the simplest difference that must be recognized is that *humans are different from other animals*. While promising research has suggested that transgenic mice (where human genes are inserted in the mouse genome) should solve these differences at least partly this does not change the fact that it's a mouse with (some) human genes. These shortcomings might lead researchers down the wrong path, eventually spending valuable resources without satisfactory result, and in some cases even harming humans [27]. Improved methods will allow the implementation of even more extensive innovations that OoC can provide. It might for example also be possible to create a device that has integrated measuring devices, making reliable intermediate data harvesting easy.

Overall it can be said that the need for reliable drug research methods is increasing, whereas there is much evidence that traditional ways are not only morally inconsistent but also harming humans in some cases. Even though it poses other challenges (such as obtaining relevant cellular material), OoC can be part of the solution to both of these problems

1.3.2. Exemplary OoC successes

Several succesful OoC-devices have already been developed. Below some interesting examples are described. Note that this list is by no means exhaustive and only shows a number of devices of interest.

The first OoC-device was the system by Huh et al. [11] demonstrating airway injuries. As mentioned in section 1.2, mechanical stresses are an important aspect of alveolar formation, but also of mechanisms such as surfactant metabolism. This is of particular interest as it reduces the surface tension epithelium [19], and deposition dysfunction relates for example to asthma and pneumonia. Huh et al studied the mechanical injury of alveolar cells caused by movement of liquid plugs. This was done using a PDMS chip with two chambers separated by a porous membrane to permit diffusion of certain particles while separating fluid and air.

Cells were cultured on the membrane in such a way that the cells are only fed cell medium from the "vessel side" and the epithelium forms accordingly (see figure 1.2).

From an engineering point of view, an important conclusion drawn by Huh et al. was that adequate perfusion of the epithelium indeed leads to a more sustainable cell layer. Having them adjacent to nutritious medium was not enough. Furthermore, it was suggested that mechanical stresses caused by liquid plug formation (as a consequence of pulmonary disease) might cause epithelial rupture. This is seen in pathologies affecting surfactant disposition, which stiffens the epithelium and makes it more prone to rupture.

This study clearly shows the benefits of OoC: options for real-time sensing, as well as a completely isolated model to eliminate external influences to obtain reliable results.

As described in section 1.2, the small intestine plays a key role in the behavior of drugs. One of the factors making it so complex to sustain an intestinal model is the microbiome. Jalili-Firoozinezhada et al. [14] sustained such a dynamic model on an intestine-on-chip supporting living human intestinal epithelium as well

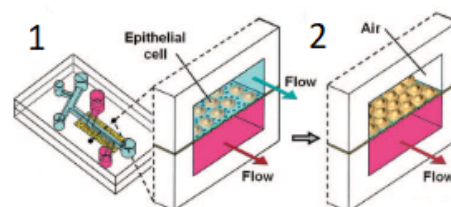


Figure 1.2: Schematic model of the Huh et al lung-on-chip. 1) Cells are grown with perfused cell medium on both sides 2) Then the top channel is cleared and an air-liquid interface is formed. Image taken from Huh et al. [11]

as a microbial population diversity similar to that seen in the human body. Like the chip designed by Huh et al., this model consisted of two chambers with a membrane between on which cells were cultured. Integrated oxygen sensors were used to maintain an oxygen gradient over the membrane. They managed to maintain the microbial culture for up to three to eight days while normally such cultures die within hours.

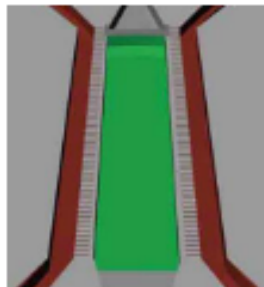


Figure 1.3: Schematic model of the Mathur et al. design with the nutrient channels (red) and cell loading channel (green). Image taken from Mathur et al. [21].

Cardiotoxicity is another major reason for drug retraction during trials - most often for cardiovascular drugs [27]. Since cardiovascular disease is the premier cause of death in the USA as of 2019 [29], this is a reason for concern. Conant et al. [6] addresses that cardiotoxicity is a major problem in cancer treatment, as chemo treatment is often detrimental to heart function. Thus, the demand for cardiotoxicity models is high.

One requirement of a cardiac model are the electrophysiological properties: cardiac potential malfunction can cause a variety of diseases. Current monolayer cell cultures are labor-intensive and often inaccurate. Moreover, the environment is not optimal to facilitate cell contraction. This can only be facilitated by formation of cardiac muscle tissue on or around certain structures. Such a design was made by Mathur et al. [21]. This had contracting cardiac muscle spanning a chamber with adjacent vasculature tubing to perfuse the system (see figure 1.3). Four model drugs were tested on this device. The tissue sustained for multiple weeks, and the response was consistent with clinical observations. Furthermore, due to the small size (a footprint of $\sim 1\text{mm}^2$), many tests can be performed in parallel allowing a high throughput.

Probably one of the most complex organs in the human body and a key factor in drug repulsion is the kidney: if the compound stays in the body for too long any adverse effects might become more severe and damage the body. Renal failure often only occurs late in the study, further increasing the need for a reliable preclinical method to predict such toxicities.

Jang et al. [15] created a model of the proximal tubule. This is the part of the renal tubules responsible for reabsorbing most of the water, nutrients and urea into the blood [19]. For this reason it is an interesting area as it is the primary spot where reabsorption, local accumulation and active clearance occur [15]. The continuous high-volume exposure makes them vulnerable to nephrotoxic substances. Here it can be seen again that a microenvironment lacking shear stress leads to a lack of local functional differentiation and eventually to insufficient *in vivo*-like kidney functions. Jang et al thus created a membrane of epithelial cells of the proximal tubule in a PDMS microfluidic system (see figure 1.4). This model showed renal epithelial functions also seen *in vivo* such as reabsorption of useful compounds. This model responded very well to active flow compared to static conditions (which are normally used in models). This is critical as, for example, a lack of glucose reabsorption is a symptom of renal dysfunction. Similarly to the model in Marthur et al, a known nephrotoxin was administered to this model. Although both models were damaged by this toxin, the fluidic model was clearly healthier after administration and recovered faster.

This model is of particular interest because it shows that even a complex organ such as the kidney can be modelled in OoC, although more steps might be needed (ie modelling all or some functional units separately).

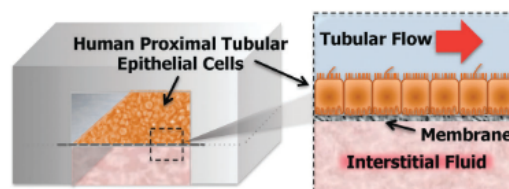


Figure 1.4: The model consists of a membrane of human proximal tubule cells cultured in an environment with physiological shear stress levels. Image taken from Jang et al. [15]

Interestingly, it can be observed that in many cases, an OoC is essentially a membrane cultured with cells of the organ in question. They all have continuous flow on either side of this membrane (fluid-fluid or air-fluid) to promote fluidic shear and thus proper cell differentiation.

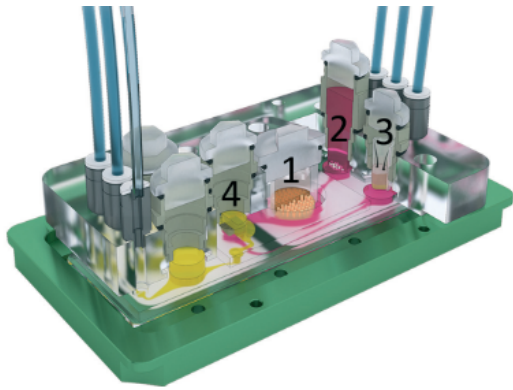


Figure 1.5: The multi-OoC developed by Maschmeyer et al., with 1) intestine, 2) liver, 3) skin and 4) kidney compartments. Image taken from Maschmeyer et al. [20]

A final exciting OoC development is the multi-organ-on-chip. Such a model was designed by Maschmeyer et al. [20], using human intestine, liver, kidney and skin cultures (see figure 1.5). An ultimate goal of OoC development is of course the 'human-on-chip', to allow for even better *in vivo*-like physiology and to study organ-organ interaction. While prior studies generally had a unidirectional flow (so no medium recirculation), this study contained a circular system. This allows for actual cross-communication between several "organs". These were chosen such that an administering organ was present (a skin biopt), a liver- and an intestine compartment connected in series in a circular system, and a kidney compartment connected to the liver part - similar to the *in vivo* structure. 28 days of stable co-culture was achieved. This is a very interesting step towards actual 'human-on-chip'-devices, even more so because of an option for external drug administration.

Concluding, OoC is a promising technique that should find its way to drug development as soon as possible. However, there are some issues that need resolving still. Firstly, development protocols currently do not generally allow medication to be marketed without animal tests [36]. To tip this scale is an issue for which human model technology needs to be proven effective thoroughly. Furthermore, all logistics and knowledge in animal experimentation is already in place, and to put someone trained to work with lab animals in a setting for OoC devices is not possible. Moreover, such workers could be reluctant to retrain because they feel their previous work and effort is disregarded by the scientific community. Moreover, working with human models requires vastly differently trained lab professionals, and researchers developing new drugs will need to design their process accordingly. These issues should be addressed as swiftly as possible in order to enable a transition in medication development to improved scientific methods.

1.4. Fluid behaviour and manipulation

Fluidic forces - literally - form a vital part of the cellular environment and in the following section some theory is explained. The first part consists of the relevant basic principles of fluid mechanics for microfluidic theory (1.4.1). Following, pump mechanism selection is described (1.4.2). The nozzle-diffuser approach is chosen as the best candidate for this particular design (1.4.3). Finally this is placed once again in biomedical context: some specific attention is given to the flow needs of certain organs (1.4.4).

1.4.1. Fluid mechanics and microfluidics

When describing a fluid, several variables can be distinguished: the velocity field [\vec{v}], and thermodynamic properties including pressure [p], temperature [T] and density [ρ]. Fluids are subject to a number of transport phenomena [30]:

- Transport of momentum: probably the most important one, as it describes the behavior of the fluid following an (external) acting force.
- Transport of mass allows mixture of different components of one flow (or for example two flows that are merged into one channel).
- Heat transport: through convection, a fluid can develop a temperature profile independent of the flow profile. As convection is negligible in microfluidic systems it is not considered here.

A fluidic system can be defined but also simplified through boundary conditions. These are in compliance with Poiseuille flow conditions [30]:

- Velocity: in case of a no-slip boundary condition, the velocity difference between the fluid and the boundary is zero. In other words, if the boundary is stationary the flow velocity at the boundary is zero. Slip does not often occur in microfluidic systems.
- Shear stress: this is sometimes known, or in case of modelling: the desired value is known. In the event of a so called 'free surface' (ie when the fluid is adjacent to a gas) it is not possible to transfer momentum

due to the discontinuous boundary layer. In this case, the shear stress at the boundary must be zero.

- Temperature: when a no-offset temperature boundary condition applies, this means the temperature of the fluid at the boundary is equal to the temperature of the boundary itself.
- Pressure: similarly, a no-offset pressure boundary condition can be applied in most cases of microfluidic systems and indicates a zero pressure difference between the boundary and the fluid.

These boundary conditions are necessary when simulating the design in order to obtain a realistic outcome, but also to avoid excessive computational effort while simulating.

When discussing the behavior of fluid flow, an essential characteristic is whether it is laminar or turbulent. Laminar flow is more continuous whereas turbulent flow is random. An easy way to determine the character of a flow is by calculating the Reynolds number:

$$\text{Re} = \frac{\text{inertial forces}}{\text{viscous forces}} = \frac{v \cdot L_{char}}{\frac{\eta}{\rho}} = \frac{v \cdot L_{char}}{\nu} [-]$$

With:

$$v = \text{Net flow velocity} \left[\frac{m}{s} \right]$$

$$L_{char} = \text{Characteristic length} [m]$$

$$\eta = \text{Dynamic viscosity} [Pa \cdot s]$$

$$\rho = \text{Fluid density} \left[\frac{kg}{m^3} \right]$$

$$\nu = \text{Kinematic viscosity} \left[\frac{m^2}{s} \right]$$

When velocities are in the order of $\frac{\mu m}{s} = 10^{-6} \frac{m}{s}$ and the dimensions in the order of millimeters, and knowing that the viscosity ν of water (one of the least viscous substances) is in the order $10^{-3} Pa \cdot s$, it is unlikely that in such a microscale the Reynolds number will ever exceed $10 - 10^{-1}$. Given that a Reynolds number below 1500-2300 indicates laminar flow, this means such systems will generally show this. With this in mind in the future some assumptions will be made [30].

Normally, in the event of an unchanging channel fully developed flow can be assumed (assuming all partial derivatives are zero), and when the forces acting on the system are constant, the flow is considered stationary. However, neither is the case for this particular design (as can be viewed in 1.4.3), remaining is incompressibility of the flow. This is valid as with expected forces and temperatures compressible behavior is unlikely.

Although many of the general principles of fluid mechanics can be applied to microfluidics, there are some issues that make one-to-one scaling of such a system inaccurate:

- As was mentioned earlier in this subsection, laminar flow will almost exclusively be observed in microfluidics.
- Diffusion is an important factor of consideration on microscale. One-dimensional diffusion can be estimated as $\hat{d} = \sqrt{2Dt}$ (the root mean square)[16]. As the distance d is squarely proportional to the time needed for a particle to diffuse over this distance, this is a significant factor in a microtube whereas it is hardly relevant in macro-sized channels.
- As the surface-to-volume ratio is much higher for smaller channels, adsorption of particles in the walls of the channels can affect testing results. Furthermore, (viscous) friction effects and heat dissipation are more significant than gravity forces.
- Surface tension might be exploited for pumping purposes in the case of very small microchannels [18]. This is what makes microfluidics unique: such mechanisms (capillary action) are much more prominent than gravity.

With this background knowledge pumping mechanism options available for this design are discussed.

1.4.2. Pumping mechanisms

In order to achieve a situation resembling the *in vivo* environment perfusion is essential. Like other mechanisms, perfusion might be passive or active. Passive mechanisms (or capillary action) utilize the liquid surface

tension and the channel surface chemical composition and texture, or more recently, the use of a hydrophilic material to generate pump action [9]. Active micropumps rely on external signals to manipulate flow [3]. Passive mechanisms are simple in nature due to their passive operation, but they are also not easily controlled and/or require complex materials. They will not be considered for this thesis. However, they might be used as design improvements.

Although external pumping devices enable high precision fluid control (using the proper equipment), there are downsides. The main one is the size: it is possible to make microfluidic devices on the millimeter scale, large pumping devices must still be coupled. Not only is this inconvenient, it also provides a critical stage with room for human error. A more fail-safe approach would be to integrate the flow manipulation segment on the chip. This way, the producer can ensure proper operation of the device to a higher degree rather than having to depend on the user for system assembly. Such devices will perform more uniformly, making test results more reliable and also possibly cheaper (since fewer samples are needed).

As mentioned above, it is necessary that the fluid flow is such that cells are properly nutrified by the medium as well as that other properties are satisfied (more on this in 1.4.4). Furthermore, it is not immediately obvious what an optimal configuration is. Several options are available:

- **External pumping options**

- Pneumatics: an external device provides a pressure gradient for pumping
- Syringe pump: a syringe is drawn in or pushed out, generating fluid flow
- Roller track: seen often in medical practice, this is a gear pushing fluid through a tube

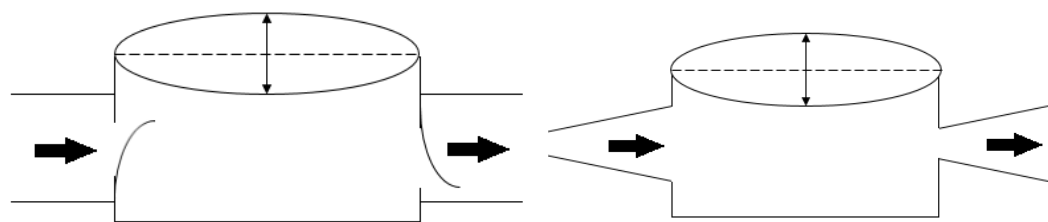
Since the intention is to use the IPMC in the micropump, a membrane-based pump is assumed.

- **On-chip pumping mechanisms**

- Flap valve membrane pumps
- Nozzle diffuser membrane pump

The working principle of the membrane pump is a moving membrane over a pump chamber. This movement causes fluid to flow in- and out of the chamber. By designing the in- and outlet of the chamber a net flow can be achieved.

Sketches of the two considered options are displayed in figure 1.6.



(a) Flap valve pump mechanism

(b) Nozzle diffuser mechanism

Figure 1.6: Sketches of the considered pump mechanisms (side views)

The flap valve mechanism is for example seen in the IPMC pump model by Nguyen et al. [24]. It consists of the following steps:

1. On an upstroke, the pressure in the chamber lowers. This causes the upstream valve to shut and the downstream valve to open.
2. Fluid is drawn into the chamber from the downstream channel.
3. On a downstroke, the pressure in the chamber increases. This causes the upstream valve to open and the downstream valve to shut.
4. Fluid is pushed out of the chamber into the upstream channel.

Although this is a well-known method, there are fabrication problems. While a set of prototypes is produced easily, an elaborate process is required for mass-production and assembly. Furthermore, moving parts are

prone to fatigue and complicate assembly.

These issues are solved when using a pumping method first described by Stemme et al. [33]: the nozzle diffuser method. This phenomenon uses the pressure drop over the nozzles to generate pump action.

The configuration of choice was a **IPMC membrane with a nozzle-diffuser channel** for the following reasons:

- This provides an excellent opportunity for the practical testing of a material developed at the TU Delft [23].
- A valveless approach solves the issues a device with moving parts has.
- The combination of an IPMC membrane and a nozzle-diffuser channel allows for a device of minimal size, therefore making effective use of resources and space on an OoC. In short, it has the potential to bring out the best in both.

As the nozzle-diffuser physics require some additional explanation, 1.4.3 is dedicated to this.

1.4.3. The nozzle-diffuser approach

This project involves a valveless channel: a mechanism using pressure differences to generate a net flow from inlet to outlet. An sketched example of such a shape is shown below. Note that the divergent side is called 'diffuser' (denoted d) and the converging side is called 'nozzle' (denoted n), given that the flow goes from left to right.

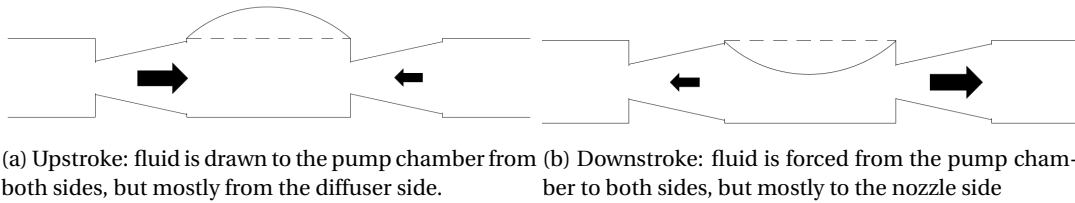


Figure 1.7: Qualitative nozzle-diffuser mechanism (side view)

Illustrated visually in figures 1.7a, 1.7b it can be seen that although there is some backflow present, still a net pumped volume is achieved. This is supported by the following mathematical analysis.

Pump action follows from a pressure drop across the nozzle-diffuser as follows [33]:

$$\Delta P_d = \frac{\rho v_d^2}{2} \xi_d \quad \vee \quad \Delta P_n = \frac{\rho v_n^2}{2} \xi_n$$

With:

ΔP = Pressure difference over the segment

ρ = Fluid density

v = Flow velocity

ξ = Pressure-loss coefficient

Then the volume flows according to Bernoulli's law are:

$$\Phi_d = A_d v_d \quad \vee \quad \Phi_n = A_n v_n$$

With:

Φ = Volume flow

A = Narrowest cross-sectional area

v = Flow velocity

As the elements are the same for nozzle and diffuser, $A_d = A_n = A$. Finally, the chamber volume variation can be described as:

$$V_c = V_x \sin(2\pi f t)$$

With:

V_c = Chamber volume

V_x = Membrane amplitude

f = Membrane frequency

t = Time

Then the net pumped volume during one pump cycle can be determined by [33]:

$$V_O = 2V_x \left[\frac{\sqrt{\eta_{nd}} - 1}{\sqrt{\eta_{nd}} + 1} \right]$$

With $\eta_{nd} = \frac{\xi_n}{\xi_d}$. This shows that the ratio η_{nd} must be larger than 1 in order to have pump action; secondly, that the larger ξ_n is compared to ξ_d , the more efficient the pump becomes.

From this a few things can be concluded:

- Pump action (or: the pressure drop) greatly depends on the resistance generated by the nozzle. Asymmetry (shown in different values for ξ_n, ξ_d) is key in generating pump action
- Membrane movement directly influences the volume per pump stroke
- Although not strictly related, they complement each other in generating pump action

What exactly affects the pressure drop over the nozzles in terms of pump dimensions is difficult to define in equations [33], and shall here be determined experimentally.

1.4.4. Flow rate in biological applications

An obvious and immediate question when designing a pumping device should then be: *what is the required volume flow?* Many articles related to organ-on-chip technology make no mention (or only a meager description) of the flow rate achieved in their device and the amount of cells depending on it. Here some suggestions are studied to determine the required flow of a pumping device.

The best way to scale an OoC depends on the purpose of the device. One or more of the following factors might be used for such scaling:

- The organ function and device purpose
- The metabolic rate of the cells in question (glucose metabolism and/or oxygen consumption)
- Fluid shear stress, which affect cell differentiation and tight junction formation
- Pulsing behavior: tissues that are supplied directly by the heart and lie inferior to the heart are more likely to "sense" heavier pulsing. In other words: the flow velocity fluctuation is higher.

It must be noted that although shear stress is what makes an OoC unique, this primarily depends on the flow rate / velocity. Thus, the focus lies on these parameters in this thesis.

Using the overview from table 1.1, the reviewed tissues are assigned relative scores to derive certain pump requirements which are used later on. Since capacity and specific properties are highly variable per study and the design is flexible even at the final stage, no specific numbers are assigned right now.

	Flow volume requirement	Flow pulsing requirement
Intestine	Medium	High
Liver	High	Medium
Heart	High	High
Lung	Low	Low
BBB	High	Low
Kidney	High	Medium
Vasculature	Medium	High
Tumor	High	Medium
Atherosclerosis	Medium	High

Table 1.2: Suggested flow properties per tissue

From this the tissues are divided in three categories:

- Tissues with the accent on high flow rate (liver, BBB, kidney and tumor)
- Tissues with the accent on pulsing flow (intestine, heart, vasculature, atherosclerosis)
- Tissues with low flow rate and pulsing (lungs)

These three types are kept in mind while designing and characterizing and reflected on in chapter 4.

1.5. Microfabrication

Although not an electronic device as those normally produced in the TU Delft Else Kooi Laboratory (EKL), the design of the intended device uses some techniques developed for the (mass) production of electronic chips. This choice was made as polydimethylsiloxane (PDMS) devices are harder to mass produce, while infrastructure for mass-production of microchips is already available in universities and industry (1.5.1). Secondly MEMS fabrication is discussed, and its relevance to the project 1.5.2.

1.5.1. Materials for biological on-chip applications

The choice for OoC materials might be made based on a number of material properties [7].

- Biocompatibility: must be in place for the material but also for bonding chemicals, if present.
- Raw material costs: not only for larger scale application but also considering prototyping
- Fabrication techniques and equipment: complexity and availability of fabrication methods limit material options
- Specific application: whereas flow actuation is considered here, it might also be applied directly to provide strain to cell cultures [10][23].

Many materials are listed as potential candidates for an OoC device.

- In the 90's early microfluidic devices were constructed from glass, silicon or quartz [7]. Standard photolithography techniques can produce microchannel networks in such materials.
- Nowadays numerous polymers are seen in OoC prototypes. The most popular one is PDMS but other options include polycarbonate, polymethylmethacrylate (PMMA) and PET [7]. They are generally formed using injection molding

Concerning PDMS, some issues are known to exist with microfluidic devices, the main one being its hydrophobicity. Since PDMS is highly hydrophobic, small molecules (such as those found in NCEs), might be absorbed into the PDMS surface [34], blurring test results. Techniques have been developed to render the surface hydrophilic (or less hydrophobic) [26] but these modifications are not permanent and have a recovery time in the order of hours to days, making the material less reliable for long-term use.

The device will be fabricated in silicon for a number of reasons. Firstly, an abundance of equipment is available at the EKL to produce silicon devices. The same is true for PDMS, but silicon avoids the issues mentioned above. Finally, it is expected that this is a more suitable choice for mass-production: production leaves very little room for human error, even when integrating other aspects in the device.

Finally a key material that is used in this design is the ionic polymer-metal composite (IPMC) mentioned earlier. This is a multilayered material consisting of a membrane of ionic polymer sandwiched between two conducting electrodes. Its deformation behavior is of special interest: it exhibits large deformation using only a low electric current (to generate a voltage difference), similarly to a piezoelectric element [25]. This property makes it an excellent actuation candidate, as high currents can lead to cell death [10]. In this sense it also differs from a dielectric actuator for OoC platforms designed previously at the ECTM group by Chuqian Zhang, as that actuator operates in a much higher voltage range.

Actuation IPMC was for example demonstrated by Nguyen et al. [24], who produced a flap-valve pump design with an IPMC diaphragm. This device was composed of a main layer of Nafion/silica and two electrode layers of Nafion, layered silica and conducting metal particles. Nafion is a synthetic polymer with ionic properties, making it very suitable for experimental electronics applications. Moreover, the material is biocompatible and operates in water (and absorbs it), making it suitable for OoC applications. It is surprising to see that there are no references of this material being used in OoC applications, which is why this will be an interesting novel take on OoC actuation.

1.5.2. MEMS technology

Micro-electronical mechanical systems (MEMS) are systems with technology on microscopical level and generally have components whose sizes are on the μm scale. Although the field has an immense amount of specialisations, some relevant basics are described here.

MEMS devices are most generally structured on silicon wafers. The silicon is semiconducting and is an abundant material on Earth which can be made from sand. Structures are then built on the substrate using

polymers (such as PDMS), several types of metal (for example for transistors) and ceramic materials. An actual device on a silicon wafer is created using a series of specific processes and materials, through additive and subtracting methods. By stacking these steps ultimately a device is formed: normally multiple ones on one wafer, which can be cut into individual chips (or 'diced'). Some of the manufacturing processes are described below:

- **Deposition** may be done chemically or physically. During chemical deposition, a gas is released on the wafer, causing atoms to be deposited. This may also be used to grow an oxide layer. Physical deposition consists of a process where atoms are released directly to form a layer of the target material. The latter allows for a smoother finish whereas chemical deposition yields a rougher surface.
- **Patterning** can be done in a **lithography** process, using a light-sensitive photoresist material that is partly covered by a mask to allow the exposed parts to be patterned. The mask may be slid in front of the wafer or, for example, a hard mask may be created using a SiO_2 layer and another patterning process. Such masks are needed when etching away material: with wet etching, the wafer is submersed in a chemical substance, whereas dry etching is done using ion bombardment (in a gas or plasma).
- **Oxidation** of a wafer can be done directly using SiO_2 deposition or it can be grown in a furnace, where the silicon is oxidized using very high temperature water vapor or oxygen molecules.

This is treated again briefly in section 5.2.

1.6. Conclusion

Due to increasing drug development costs and safety requirements, there is a great need for affordable reliable experimental testing devices such as OoC. However, low user-friendliness prevent its widespread implementation. One of the issues is related to fluid manipulation: often, an external pumping device is needed. In this chapter necessary knowledge was gathered for the design a microfluidic on-chip pumping device for OoC applications, allowing a more in-depth research statement.

Different devices have different requirements: the design shall therefore be aimed to satisfy three characteristics traits. The first is a high flow rate, the second is high pulsing behavior, and lastly a design with low flow rate and pulses.

In order to have an easy fabrication process, the chosen configuration for this pump is a membrane pump with nozzle-diffuser channels. The membrane is made of IPMC, a material with excellent properties for biomedical applications. This combination is novel in the OoC field. It may be used for example for the TU Delft Cytostretch platform [12].

In this thesis a model is designed and tested in COMSOL Multiphysics [1] to see which properties of a pump (with this configuration) lead to the desired traits.

2

Pump modelling

With the theoretical knowledge in mind it is now possible to model a nozzle-diffuser pump with a moving IPMC membrane. First a rough outline is determined for this configuration (section 2.1). The physics needed to make the model function in COMSOL are solid mechanics, creeping flow, global ODEs and DAEs and fluid-structure interaction (section 2.2). To fully define the model a parameter set is established (section 2.3). This input is taken to the COMSOL modelling workflow (section 2.4). Finally in order to fully define the starting model, literature is summarized and initial parameter values are set up (section 2.5). An overview of occurring issues and certain remarks of the modelling process is given as well (section 2.6). The chapter is summarized in the conclusion (section 2.7).

2.1. Design outline and justification

In chapter 1 the model theory was outlined. The chosen configuration is a membrane-based pump using IPMC with a nozzle-diffuser channel in which the nozzle pressure gradient generates pump action. With this in mind a very rough outline of the design can be set up (figure 2.1).

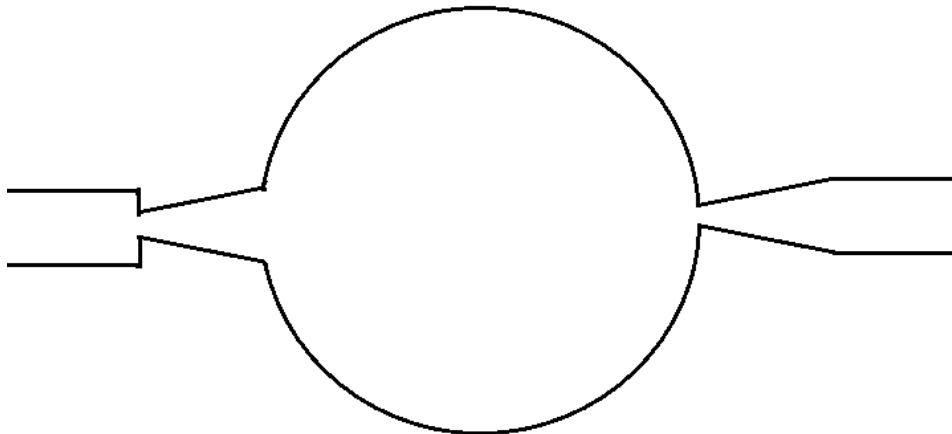


Figure 2.1: The proposed (rough) outline of the design. Note that the flow direction is left to right.

Based on the literature findings (see section 2.5), what can be seen most often is a relatively large pump chamber diameter compared to the nozzle-diffuser elements. The depth in most designs is level (ie. the same in the entire channel). No emphasis was put on the in- and outlet dimensions/shapes in any of the articles so it is assumed that a smooth transition to a wider channel will be sufficient and that the effects are small compared to the other aspects.

2.2. Physics of the model

Although the workflow is described in section 2.4, the model physics are given extra attention since defining them has been most of the work while modelling. Four physics branches are distinguished: the solid mechanics (2.2.1), the low-speed small-scale laminar flow or creeping flow (2.2.2), the differential equations to calculate the in- and outflow (2.2.3) and finally the the membrane and fluid interaction (2.2.4).

2.2.1. Solid Mechanics

An membrane was made by creating a geometrical cylinder. To the top side of the cylinder a prescribed displacement is applied, the rest of the solid mechanics model has fixed boundaries in order to reduce computation power. One free boundary is applied to the top layer of the model to allow membrane deformation. The default material for the entire structural part is Linear Elastic Material (apart from the fluidic part). All settings are kept to default but for more clarity the dependent variable names were changed to u_{solid} etc. In the middle of the membrane a harmonic displacement is applied: a sinusoidal prescribed displacement as a function of time (see figure 2.2).

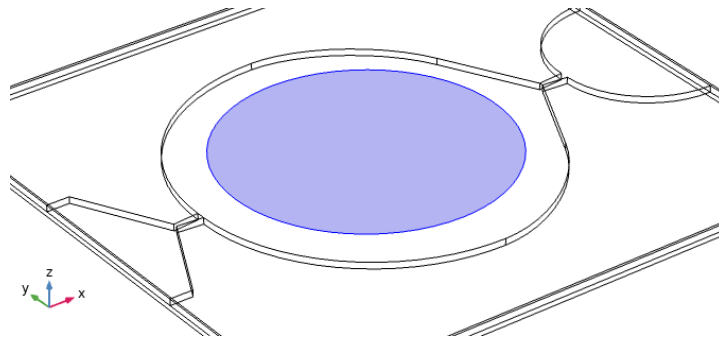


Figure 2.2: In the middle of the membrane a harmonic displacement is applied, highlighted here.

2.2.2. Creeping Flow

In order to reduce computational effort the Laminar Flow mode was changed to neglect the inertial term (ie to apply Stokes flow), which means now creeping flow is considered. This is a valid condition as it assumes viscous forces are dominant over inertial forces, which is the case at small Reynolds numbers and small flow volumes [30]. Incompressible flow is assumed (which is valid for water at room temperature) and gravity is not included due to the size of the model. Like in the Solid Mechanics module, the dependent variables were adjusted for more clarity (u_{fluid} etc.)

Most settings were left to default, initial velocities and pressures were set to zero. This is to show that there is in fact pump action when starting from a stationary fluid.

As for the inlet and the outlet, two approaches were chosen.

- At the inlet an Open Boundary condition is applied in order to allow inflow generated only by the membrane. The boundary condition was set to 'Normal stress' equal to zero, as viscous forces cannot be neglected in this case.
- At the outlet, an Outlet boundary is applied with two pressure conditions. Firstly Normal flow (to ensure outflow perpendicular to the boundary), which is valid as the flow is unlikely to be turbulent. Secondly, suppressed backflow is applied to model the real-life circular flow.

2.2.3. Global ODEs and DAEs

Two integrals were set up at the inlet and outlet. These are used in the global ordinary differential equation (ODE) and differential algebraic equation (DAE) branch in a differential equation of the form $f(u, \dot{u}, \ddot{u}, t)$. To find the time-dependent function of the net pumped volume the following equation is defined:

$$y = y' - u$$

$$V_{pump} = V_{pump_t} - U_{outNet}$$

with V_{pump_t} being the first time derivative of V_{pump} and U_{outNet} the difference between the integral at the in- and outlet. The initial values are all zero and for convenience the units are set to μl and $\mu\text{l/s}$ for dependent variable and source term respectively to avoid conversion errors later on.

2.2.4. Multiphysics

In order to be able to study the fluid-structure interaction, the fluid domain was assigned a deforming domain with fixed boundaries on all boundaries but the one adjacent to the membrane. The fluid-structure interaction was applied on the boundary adjacent to both the moving membrane and the fluid.

The coupling type chosen is Fully coupled, as the interaction is two-sided: the fluid has effect on the structure and vice versa.

2.3. Parameter identification

In order to come to a design optimum, a number of parameters were defined in order to come to a full characterization. These are divided in three categories. First these are operational parameters that can be changed after fabrication still (to some extent), being the membrane frequency and -displacement (2.3.1). Next, the chamber parameters are studied, being the channel depth and the membrane width (although the channel depth is constant throughout the device) (2.3.2). Finally the nozzle-diffuser group is studied, which are the nozzle width, the nozzle length and the nozzle angle (2.3.3). (See figure 2.3 for more clarification on the figure dimensions.)

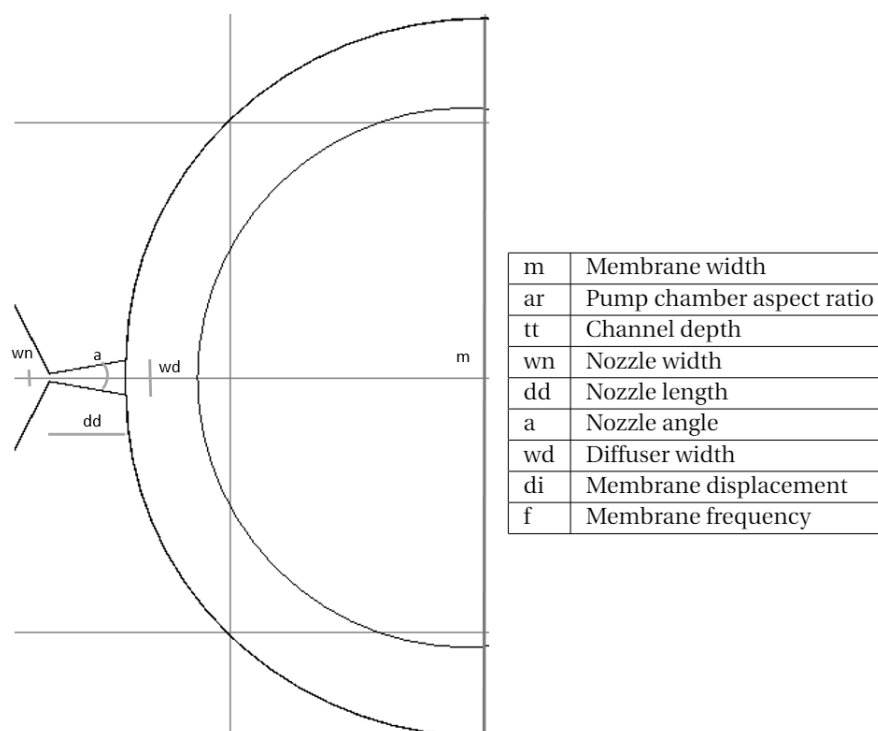


Figure 2.3: Model dimension definitions and clarifying top view for relevant parameters

2.3.1. Operational parameters

The operational parameters are membrane **frequency** f and **displacement** di . These are unique in the sense that they are somewhat flexible during operation.

Membrane **frequency** can in theory be set very high, which according to the papers in section 2.1 yields higher flow rates. However, the behavior of the material in this device is not known yet, therefore lower frequencies are studied first.

Membrane **displacement** is, as shown in appendix A, bounded by material properties but also membrane size. For the purpose of studying the characteristics of the device, this latter relation will not be taken into account at all times during simulations. Furthermore, special attention needs to be paid to the relation between the channel depth and the displacement.

The displacement is bounded by the depth of the channel, but perturbations that are too small cannot yield pump action.

2.3.2. Chamber parameters

The chamber parameters are the **membrane width** m (or chamber width) and the **channel depth** tt . Together they account for the chamber volume, and as the depth is most largely influencing the pump chamber, these are viewed together.

As mentioned in 2.3.1, the **membrane width** relates to the displacement for the same applied load (see also appendix A). In short, a larger membrane yields a larger potential displacement. It mostly affects the chamber volume and thus the pumped volume potential. It is bounded by the minimum needed displacement. There is no true upper bound but a membrane on the smaller side is preferred.

The **channel depth** relates to the membrane size in the sense that their size effects can be studied separately but together they account for volume. The depth is bounded by the required membrane displacement and by fabrication constraints: for fabrication on a silicon wafer the maximum channel depth relates to the maximum available wafer thickness.

2.3.3. Nozzle-diffuser parameters

Finally, the nozzle-diffuser dimensions are defined, the key factor in the resistance that yields pump action. Note that the converging side of a cone-shape is called the nozzle, where the diverging side is called the diffuser. The side of the pump chamber they are on are identified by in- and outlet.

All three parameters (**nozzle width** wn , **length** dd and **angle** a) (see figure 2.4) are expected to affect each other in the design. The nozzle width and angle play key roles in the fluid resistance. The nozzle as a whole might have interaction with the membrane action as well, since its forcing potential must overcome the nozzle resistance.

The angle is likely to remain small: there is not much variation in literature. Similarly, the nozzle width and length do not vary much amongst studies.

The nozzle parameters are bound by the membrane size: the diffuser width can not exceed the membrane diameter.

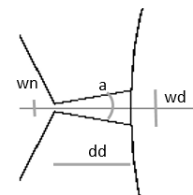


Figure 2.4: Nozzle detail with dimension variables

2.4. Modelling work flow

The model can now be set up. The modelling workflow can be found below, where the physics part is summarized only briefly on account of being treated extensively in section 2.2.¹

The modelling workflow is as follows:

1. In the global definitions, all geometrical dimensions are defined, including some dependent variables (such as the diffuser width which depends on the nozzle width, length and angle solely). The relevant ones are listed in figure 2.3 and the accompanying table.
2. The model geometry (figure 2.5) was made based on literature findings as described in section 2.5 and initial values described in section 2.1. It can be divided in six domains: four structural domains for the stationary parts of the system, the fluid filling the channel, and the flexible membrane covering the top.
3. The model contains three materials (water, silicon and PDMS). Although the membrane in the intended design is not made of only PDMS, it is sufficient for the simulation purpose: to gain insight in the physics principle of the valveless pumping mechanism.
4. The physics are assigned as described in section 2.2.
5. In the component definitions two integrals were applied: one on the outlet and one on the inlet. This performed an integration on the respective boundaries, yielding the flow velocity magnitude. The difference between the two was defined as U_{outNet} , which is the input for the differential equation needed to calculate the flow rate.
A deforming domain was defined on the fluid domain, with fixed boundaries on all sides except the fluid interaction boundary.
6. Finally a mesh was applied to the model. Since the fluid is the most important part to be studied this was meshed first, in a coarse mesh calibrated for fluid dynamics. The structural elements all had coarse elements for general physics.

¹Prior to this model, a 2D model was designed in order to verify that the mechanism would show pump action, which it did. However, as this was merely an example to practice with, it has not been included in this thesis.

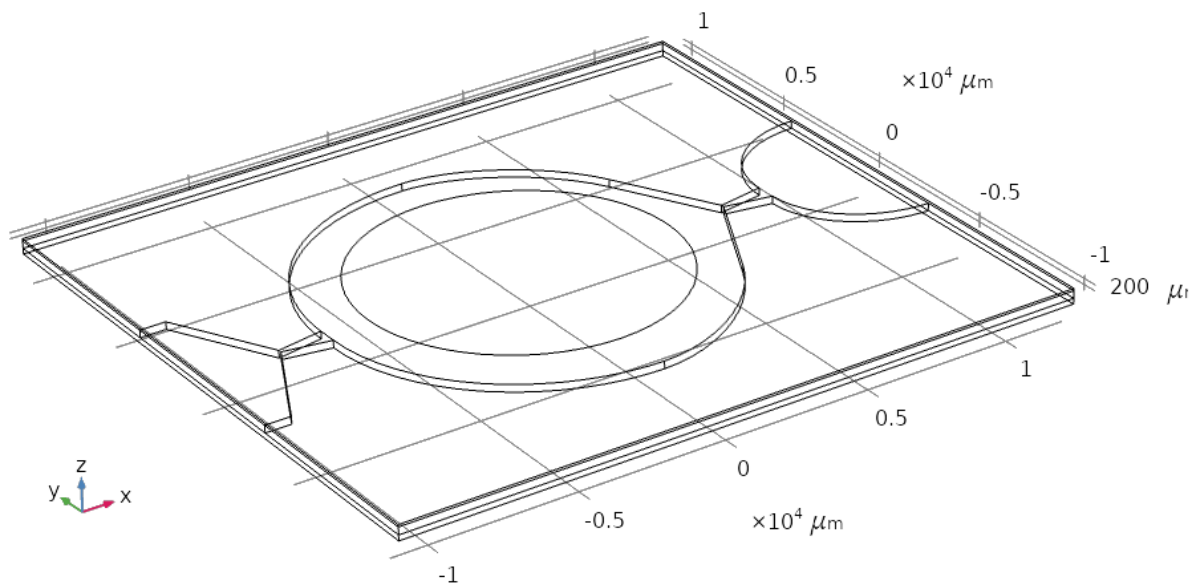


Figure 2.5: Isometric view of the model geometry

2.5. Initial design: literature background

The model is now fully defined by looking more closely at examples from literature. Below selected publications used as inspiration in the design are summarized with their technical details of interest (table 2.1).

	Chamber volume	Nozzle diameter, angle and length	Frequency / displacement	Maximum flow rate, back pressure	Other remarks
Stemme [33]	141.8* μl	A: 230 μm , 20°, 4mm B: 530 μm , 10.7°, 3mm	A: 110Hz, 12.5 μm B: 310Hz, 13 μm	A: 2250 $\mu\text{l}/\text{min}$, 11.7kPa B: 7500 $\mu\text{l}/\text{min}$, 0.5 kPa	In this study, model A was more efficient (energy per stroke).
Yamahata [39]	19.24 μl	100 μm , 9.5°, 2.3mm	12 Hz, 200 μm	200 $\mu\text{l}/\text{min}$ at 600 Pa	
Nguyen [24]	15.39 μl	This is a flap-valve design	3Hz, 150 μm	760 $\mu\text{l}/\text{min}$, 1.5kPa	The performance was studied for various voltages, the optimum was 3V.
Cheng [4]	5.53 μl	80 μm , 10°, 1.28mm (only inlet)	10kHz, -	1.10 $\mu\text{l}/\text{min}$, 16.7Pa	This is a 3D pump with three inlets and one outlet.
Zhou [40]	17.3 μl	100 μm , 10°, 1.6mm	36.9Hz, 34.34 μm	319.6 $\mu\text{l}/\text{min}$, 850Pa	
Singh [32]	30.8 μl	120 μm , 10°, 1.5mm	200Hz, 1 μm *	20 $\mu\text{l}/\text{min}$, 220Pa	The study shows about -10% difference between simulations and experiments, likely due to energy losses.
Kawun [17]	5.65 μl	86 μm , 10°, 0.95mm	12Hz, 450 μm *	135 $\mu\text{l}/\text{min}$, 245 Pa	Although sharp angles optimal in nozzle-diffuser configuration, this had round angles due to milling constraints.

Table 2.1: Design specifications of models and products. Often, multiple output values were named: only the highest output parameters are mentioned here. Numbers marked with (*) were not specified in the article (or one or more numbers to calculate it were missing) or were otherwise unclear, and those were therefore estimated based on illustrations and/or other dimensions.

It should be noted that there are many examples of nozzle-diffuser micropumps (and this list is by no means exhaustive). Moreover, not all examples are micropumps specific to OoC devices. The draft design in this thesis will be a mixture of several techniques using characteristics from several designs.

A number of things can be learned from these articles.

- Most current designs use electromagnetic actuation. Only a few use a piezoelectric element.
- Most designs use a high frequency and relatively low displacement.
- When comparing chamber sizes, Nguyen outperforms the others by far, pumping almost 50 times the chamber volume per minute. Cheng and Singh have a much lower score, pumping less than once of the chamber volume per minute. It should be noted, however, that Singh has a relatively large pump chamber volume.
- Nozzle-diffuser element dimensions are quite similar for the selected designs.

With this in mind, some initial values are set up for the design (see also figure 2.3). These are based on common occurrences in the selected articles. It must be noted that these values need not to be optimal, they are an initial guess at a design that will provide some first results.

- To accommodate the small size the design strives for the membrane dimensions of Singh et al. [32] are adopted. This is an interesting design is due to the fact that it was tested with an asymmetric pump chamber which provides a smoother fluid exit. **The membrane diameter is set to 14 mm.**
- Likewise, **the channel/chamber depth is set to 250 μm .**
- The nozzle-diffuser parameters are mostly similar: **the nozzle width is 150 μm , the nozzle angle 10°, the nozzle length 1.5mm.**
- Since not much is known about the IPMC performance in this setting, a low initial frequency is chosen. **The frequency is 3Hz.** Literature shows frequencies of at least 10 Hz can be achieved [24][23] a lower testing frequency is chosen to be on the safe side.
- The membrane displacement depends on the material properties (see appendix A). **The membrane displacement is 40 μm .** This might not be the maximum achievable displacement but it will be considered as such for the purpose of characterizing the system.

2.6. Discussion and iteration

During modelling, some issues and remarks came up that are listed below.

- For the in- and outlet of the channels, two options are available in terms of physics selection: inlet/outlet or open boundary. To choose the outlet option at the outlet side backflow can be prevented and is a more realistic situation as the flow in a test setup will be circular, providing some momentum which indeed prevents backflow.
- Some (computational) time might have been saved by treating the channel walls as boundaries rather than "carving out" the channel in a solid block.
- A dedicated mesh size for individual domains is beneficial over a one-size-fits-all approach.
- It was beneficial to apply Creeping flow rather than Laminar flow in terms of computational power.
- A lot of time was spent on getting the global ODEs and DAEs right. If the background had been studied in more detail this could have been avoided.
- A major problem was encountered when many results returned errors, making the modelling process increasingly difficult. This was solved by changing the settings for the Jacobian update from 'minimal' to 'on every iteration': in the former setting solutions would often not converge leading either to an error or an infinite loop and unworkable situations during simulation. This greatly increased computational effort but it did ensure that most nodes returned a result, which made postprocessing a lot more easy. It again emphasized the need for minimum computational effort on other aspects.

All in all it can be said that the model is working properly and will, after verification, enable good modelling of a real-life situation.

2.7. Conclusion

In this chapter the process from literature, to initial values, to the working model was described. A multiphysics model was made in COMSOL Multiphysics of a 3D model using solid mechanics, creeping flow, and fluid-structure interaction to review its performance. This enables simulation of the characteristics of a nozzle-diffuser pump with and IPMC membrane. The issues and iterations were discussed for the readers' reference as well.

3

Simulations

In this chapter the simulations are executed and the model is characterized. First some verification steps are performed: the membrane eigenvalue is estimated and laminar flow conditions are checked (section 3.1). After this the model characterization process is described (section 3.2). The results of this process are presented after this, starting with the independent parameter studies (section 3.3). These are summarized in an intermediate findings section, setting expectations for the next part of the study (section 3.4). These are followed with six interaction studies for parameter pairs that are expected to have shared influence on the model (section 3.5). Finally a double-nozzle configuration is tested as an alternative to the model used in the rest of the chapter (section 3.6). The chapter is summarized in the conclusion (section 3.7).

3.1. Model verification

The model was fully defined in section 2.5. Before the model is characterized some verification steps are performed. The eigenvalue of the membrane-fluid interaction is estimated so that the design might benefit from resonance properties (3.1.1). In order to verify the laminar flow assumptions the velocity development is studied and the Reynolds number is calculated (3.1.2). With this in place the simulations for model characterization can start.

3.1.1. Eigenvalue analysis

An eigenfrequency analysis is performed, as the resonance frequency is often a good candidate for a frequency optimum. If this is within the expected operating range it might be considered.

The (first) eigenfrequency of a clamped cantilever beam (for clarifications on this particular assumption see appendix A) is defined as [22]:

$$f_1 = \frac{1.758}{\pi} \sqrt{\frac{EI}{mL^3}}$$

With:

EI = The cantilever bending stiffness [Nmm²]

m = System mass [kg]

L = Beam length [mm]

According to Stemme et al. [33], in a system like this, the mass m can be defined by the mass of the volume in the pump chamber (since the membrane is, by comparison, very low in weight).

Note that the variable m was used for the membrane width previously (and again in the next equation).

$$f_1 = \frac{1.758}{\pi} \sqrt{\frac{EI}{\rho \left(\frac{m}{2}\right)^2 t t \cdot \left(\frac{m}{2}\right)^3}}$$

With:

$$\begin{aligned}
 EI &= \text{The cantilever bending stiffness [Nmm}^2\text{]} \\
 \rho &= \text{Density of water [kg/mm}^3\text{]} \\
 m &= \text{Membrane width [mm]} \\
 tt &= \text{Channel depth [mm]}
 \end{aligned}$$

And so:

$$\begin{aligned}
 f_1 &= \frac{1.758}{\pi} \sqrt{\frac{0.1625}{3.848 \cdot 10^{-8} \cdot 343}} \\
 &= 197[\text{Hz}]
 \end{aligned}$$

This is a frequency well above the range that will be studied. It is unlikely that with changing parameters the resonance frequency will near that range. According to this computation it is not likely that the benefits of resonance can be reaped in this design. Things that would lower the natural frequency are: a denser pump fluid, a deeper channel, an increased moment of area (mostly by increased membrane thickness) or increased membrane size.

3.1.2. Laminar flow

In order to ensure that the extracted data is reliable it must be verified that the flow indeed is laminar. An easy way to identify laminar flow is to calculate the Reynolds number. The critical variable here will be the flow velocity, or rather the local maximum velocities. With this in mind, the following steps are taken:

- Calculate the Reynolds number as a function of the variable velocity, determine the threshold for transient flow (at $Re=2300$);
- Identify the points at which prominent flow velocity peaks occur;
- Evaluate the flow velocity in these points over time;
- Verify that the threshold is indeed not crossed

The definition of the Reynolds number is as follows [30]:

$$Re = \frac{\rho v L}{\mu} [-]$$

(See also 1.4.1) Note that for this case the characteristic length (the nozzle width) is constant but in other settings it can be a variable. Assuming the channel fluid is always water and that a Reynolds number below 2300 is desired, the equation is rewritten to:

$$\begin{aligned}
 \frac{1000 \cdot v \cdot L}{8.9 \cdot 10^{-4}} &\leq 2300 \\
 v \cdot L &\leq 2.047 \cdot 10^{-3} \left[\frac{\text{m}^2}{\text{s}} \right] \\
 v \cdot L &\leq 2.047 \cdot 10^3 \left[\frac{\text{mm}^2}{\text{s}} \right]
 \end{aligned}$$

Note that the last step is taken to avoid conversion errors: the unit of the right-hand side is converted to $\frac{\text{mm}^2}{\text{s}}$ so that the velocity might be entered in mm/s rather than having to convert to m/s. The characteristic length is also entered in mm.

It now seems that it is unlikely that this design will see transient flow: with the current throat size being only 0.1 mm, local velocities in the order of 10^4mm/s are needed to reach this state. Nevertheless, it is good to verify this and to look at the velocity profile.

This flow has a no-slip condition, meaning the wall velocity is equal to the flow velocity at the boundary (in this case zero). Following from this it can be deduced that for each yz-cross-section of the channel the maximum flow is found at the exact center of the channel, as this is the point with the largest distance from all nearest walls [30]. With this in mind, in the COMSOL model a 'Cut line 3D' is generated, which passes exactly through the centroid of the channel section and is parallel to the x-axis (figure 3.1).

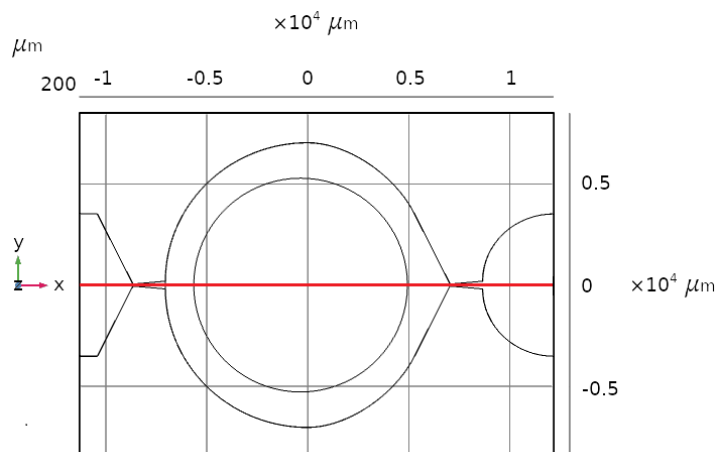


Figure 3.1: Top view of the model with the cut line shown in red

The flow velocity magnitude is not symmetrical from this plot: only the peaks just upstream of the nozzle throat. This could be due to special upstream flow properties, but it might be a computational error. However, as the peaks are not excessively high, this is not an urgent matter to attend. On this line the flow velocity magnitude can be evaluated at all time steps (figure 3.2). Note that no legend is shown, since only the location of the peaks are relevant at this moment and not the time they occur.

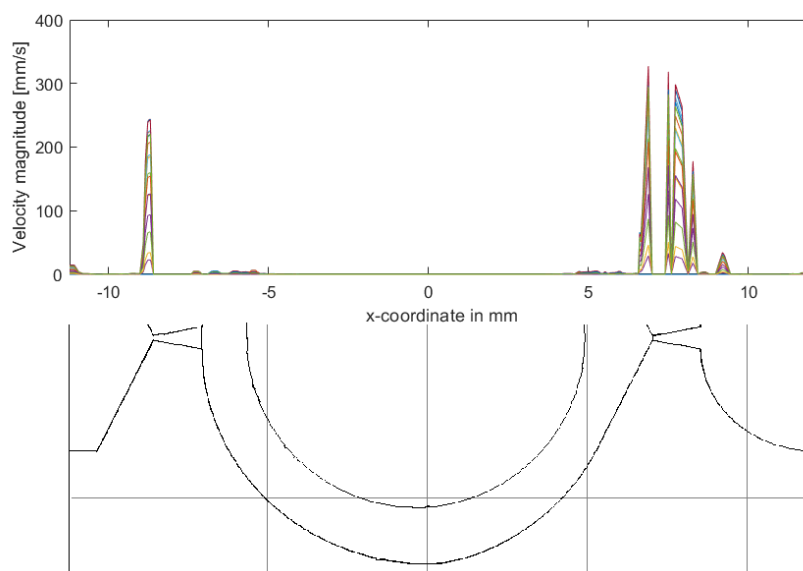


Figure 3.2: Velocity profile of the flow rate at several time steps, displayed in relation to their position in the model.

Based on this plot, several large peaks can be observed, mostly around the nozzles (which was to be expected). Although there are more local maxima than these, any overall maximum velocities are likely to occur in one of these peaks. There are several local peaks in the outlet nozzle, which might lead to think that there is actually turbulent flow here, although the velocity magnitude is too low for that.

It is notable that the maximum is not in the throat of the nozzle, which one might expect intuitively: for an incompressible flow, the volume flow is constant in a steady channel flow. However, this is not a steady flow (it is a function of time [30]).

Based on this dataset, it can be concluded that if the flow is laminar in all of these maxima, it is laminar in the entire model. For this reason these points are studied further.

Using the Matlab function `findpeaks` and the argument `MinPeakProminence`¹ five relevant maxima are

¹to find only certain prominent maxima, namely those with a prominence of at least 100 mm/s compared to neighbouring peaks

identified. These locations are located in the Comsol model, plotting the expected peak locations as a function of the model size (which will be varying further on in the optimization process). They are plotted using Cut Point 3D and all lie on the line determined earlier (figure 3.3).

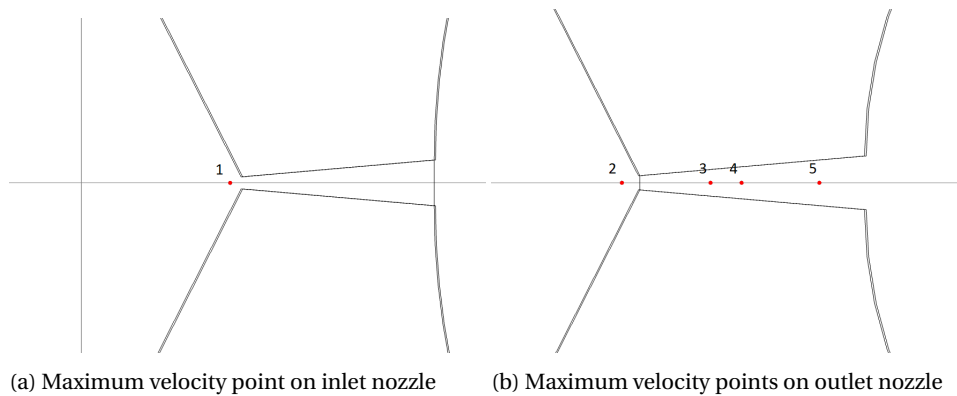


Figure 3.3: Top view of the nozzles with the cut points shown in red

The flow velocity development in the points found above is evaluated in COMSOL and plotted below (figure 3.4). For this a sample time of 2.5 seconds and a decreased timestep of 0.1s was taken to be sure to capture the full spectrum of velocities.

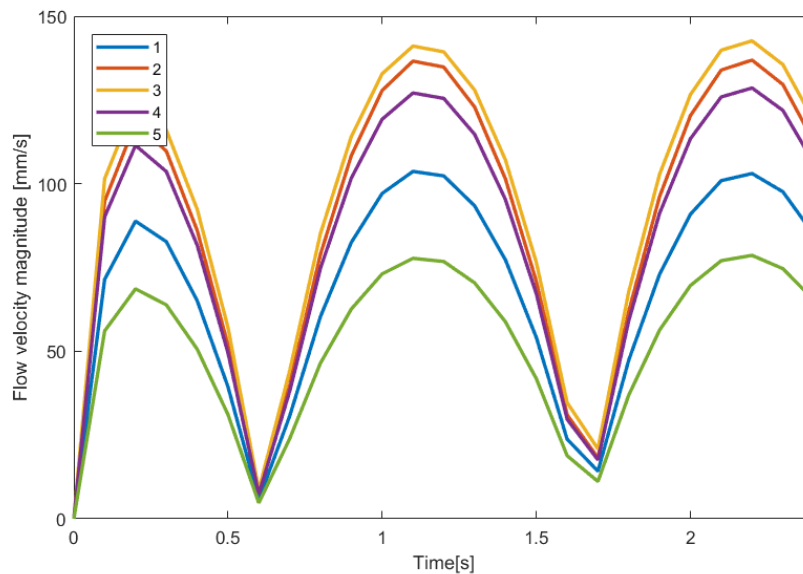


Figure 3.4: Flow velocity in selected points. Refer back to figure 3.3 for the exact locations of these points.

The maximum values occur around the outlet nozzles: the two maximum values are before and after the outlet nozzle throat. From this it can be observed that the Reynolds number never exceeds the turbulence transition threshold in the base model, and is not likely to do so for the expected range of values. The check-point for this must be after one or two cycles, after which this is fully developed. Another peculiar thing that is seen here is the cycle frequency: although the frequency of the membrane in this simulation run is 3Hz, the velocity cycle frequency around the nozzles is about 0.9Hz. This is investigated in 3.3.2.

3.2. Model evaluation and characterization process

The current model is one with many variables and interesting behaviors. In order to extract proper results from the model, a number of steps are described below.

3.2.1. Base model evaluation

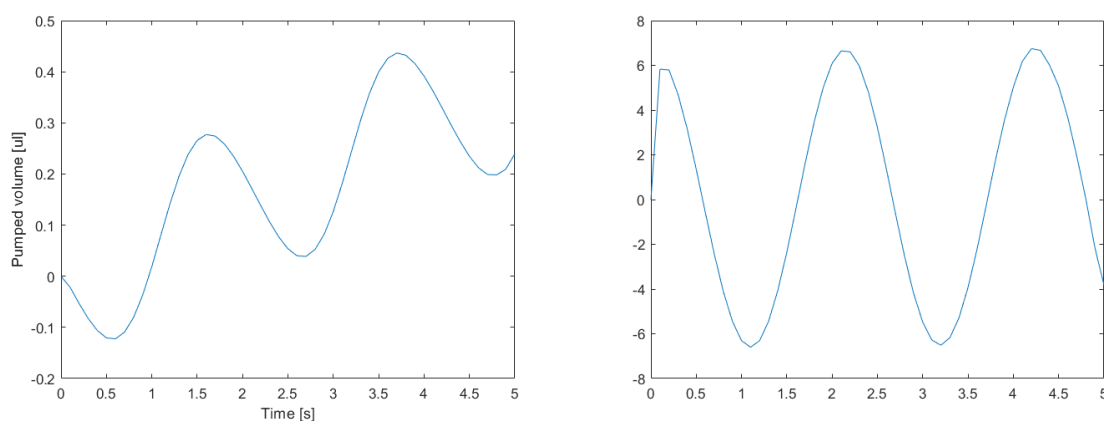
In order to characterize the model and evaluate the influence of the parameters, certain data is extracted from the model. This is tested using three criteria:

- **Model flow rate:** the flow rate per minute provides a measure of the effectivity of the model. It is calculated by COMSOL by calculating the difference between the integral inflow and outflow at the given time steps and then solving the differential equation $V_{pump_t} - U_{out_{Net}} = 0$ (see 2.2.3), after which the pumped volume is extrapolated in Matlab to find the flow rate.
- **Outlet fluid velocity:** depending on the application, a more continuous or a pulsating flow is desirable. The pressure at the outlet (as a function of time) provides an indication of this 'pulsating' behavior.
- **Velocity profile:** as there are several changes in channel shape throughout the device, it is relevant to study local velocity peaks. Although the intention was to create a velocity profile for a range of dataset, during simulations it became clear that this data could not be exported for processing due to unclear issues and thus drawing meaningful conclusions was not possible.

This is first done using the base model defined by the initial values (see section 2.1). Furthermore, in order to determine a certain minimum sample size for which reliable results can be extracted but also minimal computational effort is required, a data point analysis is performed. This is done based on the results from the flow rate (see 3.2.2). For the initial evaluation an arbitrary sample time of 5 seconds was chosen. As a time step, it seemed fitting to look into control theory: a time step following the Nyquist sampling theorem should grasp all waves initiated by the applied frequency. This means a timestep of at least $\frac{1}{2f}$ with f the applied frequency is used.

Below the above extracted plots are given for the base simulation. Note that only the plots of particular interest are displayed here (with some additional ones in appendix B). Some of the Matlab scripts used for postprocessing are found in appendix C.

The first plot of interest is the pumped volume as a function of time (figure 3.5a). The pumped volume is extrapolated to calculate the flow rate using the Matlab function polyfit. From this a flow rate of **4.59 $\mu\text{l}/\text{min}$** was found. Here, too, it can be seen that after one flow cycle the development is quite steady. The same phenomenon as in 3.1.2 is observed here: the flow cycles are not occurring at the same frequency as the membrane frequency. The net pumped volume has the form $t \cdot \sin t$.



(a) The base pumped volume as a function of time.

(b) The flow velocity at the outlet boundary.

Figure 3.5: Base model configuration flow development

Secondly the outflow behavior is studied. This is used as a measure for the pulsing behavior of the flow (figure 3.5b). Like the pumped flow this plot shows pulsating behavior. What stands out is that although the

flow rate is about $4.5 \mu\text{l}/\text{min}$, the flow amplitude at the outlet is almost $4 \mu\text{l}$ per cycle. This implies that the pump is pulsating heavily: on each cycle, the pumped volume is only about 15% of the total moved volume.

Finally, for the velocity profile, please refer to the plot in 3.1.2 (figure 3.2 and 3.4).

3.2.2. Initial characterizations (process)

Prior to finding the optimal solution(s) for this design, insight is gained in the influence of the parameters determined earlier (see section 2.3) but also the required sample time and time step size. If in any case it appears that a parameter shows a clear maximum or another obvious sign that the current one is not a good choice, it might be decided to chance this variable for the rest of the process.

The following steps are taken:

1. **Sample time:** in sample runs it has been observed that the outflow period is not entirely predictable, and therefore an estimate should be made that can apply to future models. An attempt was made to make calculations based on one flow cycle, however, this is not always applicable as sometimes the pumped volume is a sequence of steep parts and plateaus, rendering such an approach useless. A better one-size-fits-all approach is to make a tradeoff between computational effort and accuracy and use this, while keeping the discrepancy in mind.

To do this, the following steps are taken (see also appendix C.1).

- Perform a full simulation run is performed from 0 to 60 seconds with the base model
- Recognize that the pumped flow at 60 seconds is equal to the flow rate in $\mu\text{l}/\text{min}$
- Calculate flow rates based on partial data sets using the first 1, 2, 3... datapoints
- Compare these partial extrapolations to the true flow rate
- Determine which number of samples provides a sufficiently accurate flow rate while keeping the sample time at a minimum value

This number of samples is used in further runs.

The two **operational parameters** are studied now.

2. A frequency sweep (with the membrane frequency) performed. In order to satisfy the the $\frac{1}{2f}$ maximum step size this is a variable too.
Meanwhile, the effect of the frequency on the flow rate and the local velocity profile is studied as well.
3. A displacement sweep is performed. It should be noted that a wide range is used here, although this is in reality limited by the membrane size (see appendix A).
4. If changes have been made in steps 2 and 3, an iteration is made, starting from step 1.

The next parameters to be studied are the **chamber parameters**.

5. A membrane width sweep is performed. The displacement for this run remains constant.
6. Two channel depth sweeps are performed: one where the displacement remains constant and one where it scales with the channel depth. This separation is made to eliminate a possibly influence from the displacement being percentage of the channel depth.

Finally the third segment, the **nozzle-diffuser parameters**, is treated. These are performed in order of expected significance.

7. A nozzle angle sweep is performed.
8. A nozzle throat width sweep is performed.
9. A nozzle length sweep is performed.

Note that both nozzle-diffuser elements, at both inlet and outlet, are varied the same way. To the best of the authors knowledge, there are no studies that are similar to this one that have different dimensions for inlet and outlet elements.

These are the initial characterization runs. Aside from step 4, other iteration might be performed if the situations calls for it.

3.2.3. Interaction characterizations (process)

After the initial characterization is completed, some interaction studies can be performed. These mainly concern the flow rate output as to not add to many variables to the study.

The following interaction studies are expected to be of interest:

- **Membrane frequency and displacement.** This interaction is relevant as they both can be changed during operation.
- **Membrane width and channel depth.** As these effectively determine the chamber volume, some special attention is paid to which one is most influential in the output.
- **Membrane displacement as a function of membrane width.** Taking into account the limitations of the membrane material the output might change.
- **All three nozzle-diffuser parameters.** Three interaction studies are done for this subset to see if one is particularly significant (and if yes, which one).
- **The most significant nozzle-diffuser parameter and membrane displacement.** As the nozzle element acts as a damper/resistive element, an optimum combined with the membrane displacement might be seen.

3.2.4. Alternative configuration

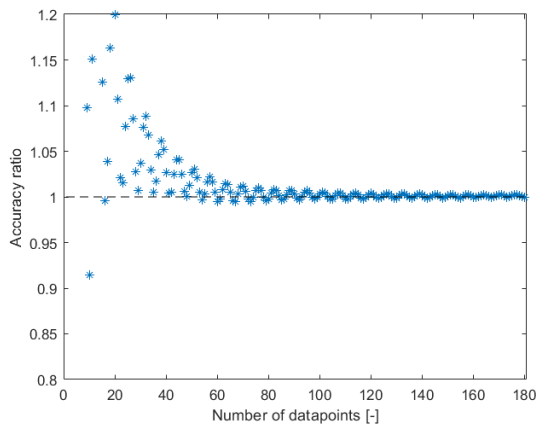
An optimized model can be used to construct an alternative pump configuration to compare to the standard model. This is the double nozzle setup (in series, on either side of the membrane). Ullmann et al. also described a number of possibly interesting configurations [35].

3.3. Initial characterization (results)

In this section the results of the the initial characterization process are described as described in section 3.2. Note that due to the large amounts of changing variables, with each plot a table with the current values is given so the reader can keep track of this.

3.3.1. Sample time

As a starting point, an estimate for an accurate **sample time** was made (see 3.2.2). The results can be viewed in figure 3.6: these are the extrapolated flow rates found when taking the results from the first n data points only, compared to the true flow rate.



t	60s	tt	250 μm
Δt	0.3s	a	10°
f	3 Hz	wn	150 μm
di	40 μm	dd	1.5 mm
m	14 mm		

Figure 3.6: Accuracy ratio for time samples taken cumulatively from 1 to 180 datapoints. Note that $t=0$ is excluded and that the plot only displays accuracy ratios between 0.8 and 1.2.

It can be seen that only from 40 datapoints the extrapolation values are consistently within a 5% error margin. (This corresponds to a sample time of about 13 seconds.) As simulations are computationally expensive, this sample time is not a workable situation.

In order to choose a suitable sample size, some boundaries are set:

- An accuracy between 0.9 and 1 is sought: to underestimate the flow rate is less risky when qualifying pump performance.
- To keep the computational time in check, there should be no more than 20 datapoints total, but still the largest possible amount within these bounds.

There are two values satisfying these criteria: $n=11$ and $n=17$ (or, in this case, $t=3.333s$ and $t=5.333s$), with an accuracy of 91.4% and 99.5%. To be on the safe side, 17 datapoints are chosen. This sample size is taken to the operational parameter analysis.

3.3.2. Frequency

As the flow output is greatly influenced by the membrane frequency, this is treated first. It might also affect the sample size requirement.

The time step was variable to ensure inclusion of all points of interest in the result: $\frac{1}{2f}$. To get to 17 datapoints the sample time was set to $\frac{17}{2f}$. The flow rate development is found in figure 3.7.

It is unclear what frequency magnitudes can be reached for the IPMC setup and for this reason the focus lies on the lower frequency range.

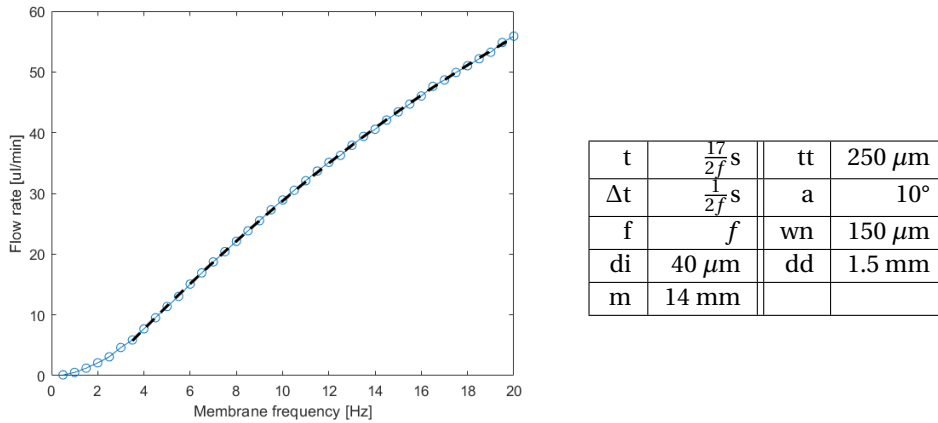


Figure 3.7: Flow rate output as a function of frequency. The dashed line indicates the fitted curve for the frequencies above 3.5 Hz.

The full data plot can be found in figure B.1. The flow rate as a function of frequency follows a parabolic curve starting from $f=3.5$ Hz. Contrary to what the model of Nguyen et al. shows, there is no maximum seen here. In that study a maximum was found for driving frequencies of 3 to 5 Hz and these also lead to smaller membrane displacements - however, these were also very high flow rates considering the model size. This can probably be attributed to that the applied membrane displacement is larger, and secondly that the flap-valve system has a more efficient flow output.

The pulsing behavior can be viewed in figure B.2. Furthermore, as was addressed in previous sections, the relation between membrane frequency and flow frequency is not quite clear yet. The plot addressing this relation is displayed below (figure 3.8).

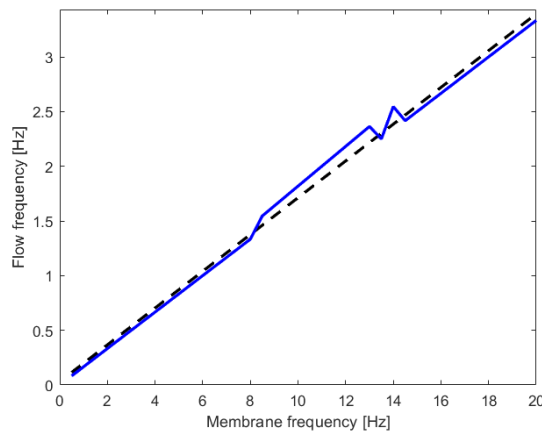


Figure 3.8: Membrane frequency versus outlet flow frequency. The dash line indicates the fit $f_{out}=0.1681f_{in}+0.0312$ [Hz].

From this it can be seen that the relation between the membrane frequency and the outflow frequency is almost completely linear, the irregularities in the middle are small.

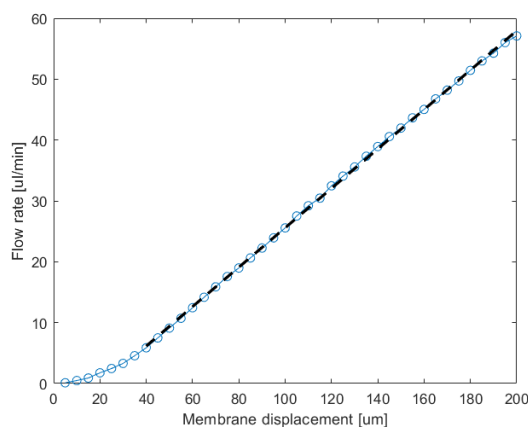
The frequency shift can be explained by the nozzle and the pump chamber: these act as a damper and as a consequence of damping as well as the shift of fluid movement direction the membrane frequency does not translate directly to the outflow frequency.

To take a smaller time step is not needed for now.

3.3.3. Displacement

The last step of the operational parameter sequence is the membrane displacement, the plots of which are displayed below (figure 3.9).

The testing range was intended to go from $5\mu\text{m}$ to $250\mu\text{m}$, however, the final values ($205\text{-}250\mu\text{m}$) returned only errors. This could have been caused by the fact that this displacement stretches the membrane too much or that the displacement converges to the bottom of the channel.



t	2.43s	tt	250 μm
Δt	$\frac{1}{7}\text{s}$	a	10°
f	3.5Hz	wn	150 μm
di	<i>di</i>	dd	1.5 mm
m	14 mm		

Figure 3.9: Flow rate output as a function of membrane displacement. The dashed line indicates the fitted curve for the displacements of $40\mu\text{m}$ and higher.

The flow rate development is almost perfectly linear throughout the range of displacements. It is expected that the limit is $di = 250\mu\text{m}$, the depth of the channel, with the maximum flow rate just before that. The linear development starts from around $40\mu\text{m}$ or 16% of the channel depth.

As the frequency changed, an iteration of steps 1-3 is performed to make sure the results are not affected (much). This yielded a slightly larger sample size. The other parameter sweeps did not differ significantly (less than 5%) and so the values are kept this way.

Following this is the analysis of the **chamber parameters**.

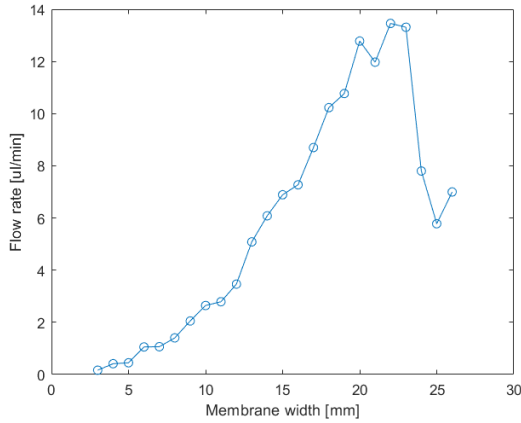
3.3.4. Membrane width

Firstly the membrane width is the variable parameter. The flow rate development is displayed below (figure 3.10). A testing range to at least a 30 mm membrane was intended, however, at a certain point no solutions were returned by the model anymore for unclear reasons.

The flow rate does not develop as predictably as the previous parameters did. Since the flow rate at 14 mm is quite low, it is increased slightly to gain more pronounced results in future runs. However, the software was clearly struggling on the higher parameter segment, where the simulation time needed increased dramatically per m .

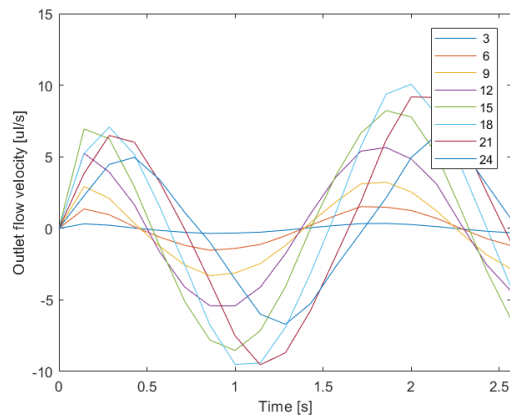
This dataset shows that there is a certain 'efficiency maximum' to the flow rate development. After this the membrane movements are likely too small to introduce significant fluid movement.

More interesting developments are seen in the outlet velocity. Like the flow rate, this reaches a maximum around $m=20\text{mm}$. Moreover, the flow frequency seems to change with varying membrane width (see figure 3.11a and 3.11b). Note that on figure 3.11a, not the entire range of tested parameter values is displayed.

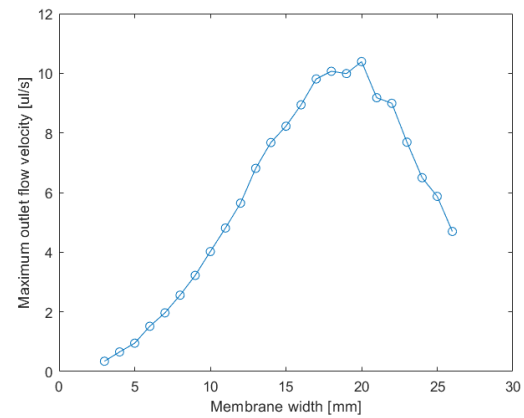


t	$\frac{18}{7}$ s	tt	$250 \mu\text{m}$
Δt	$\frac{1}{7}$ s	a	10°
f	3.5 Hz	wn	$150 \mu\text{m}$
di	$40 \mu\text{m}$	dd	1.5 mm
m	m		

Figure 3.10: Flow rate output as a function of membrane width.



(a) Outlet flow velocity development



(b) Maximum outlet flow

Figure 3.11: Outlet flow velocity for varying membrane width

Using a similar procedure as in 3.3.2, however, no significant differences were found. This can be subject to a future study, with a larger sample size and a smaller time step. From visual inspection, it seems as if the frequency becomes higher and higher up to a certain point (around the maximum of the outlet flow), after which it decreases again. This might be related to the shift seen in the frequency sweep: the volume under the membrane acts as a buffer, and when this buffer is too large the flow rate efficiency drops again. This development is more or less consistent with the findings of Singh et al, who used very similar dimensions [32] (see also section 2.1)

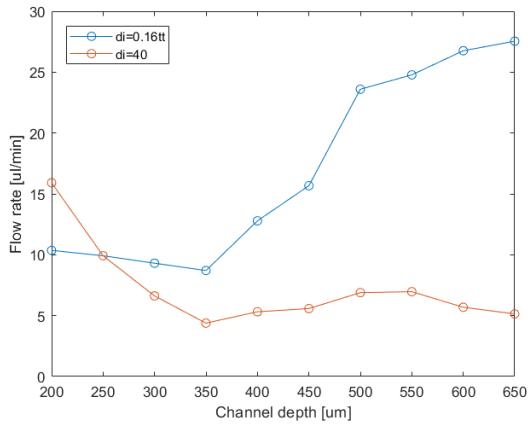
To still have some advantage to the more pronounced flow rate without sacrificing too much computational effort, m is increased to **18mm**.

3.3.5. Channel depth

Secondly, the channel depth tt is tested. This was done in two ways: while keeping the absolute membrane displacement di constant, and while keeping the relative membrane displacement constant (ie. at 16% of the channel depth). The resulting flow rate output is displayed below (figure 3.12).

The range of channel depths was based on the maximum possible channel depth (in a wafer of $700\mu\text{m}$). The minimum depth was intended to be lower than $200\mu\text{m}$ but these yielded errors. The influence of the relative displacement of the membrane compared to the channel depth is undeniable: while the "16%"-line has an overall rising trend, the " $40\mu\text{m}$ "-line drops immediately and remains steadily low. Another thing is the seemingly critical area between 350 and $500\mu\text{m}$. This is something to look into when studying the interaction between the membrane width and channel depth: possibly the membrane width relates to this "jump".

Next, a comparison can be made between the maximum outlet flow of the two cases (see figure B.3).

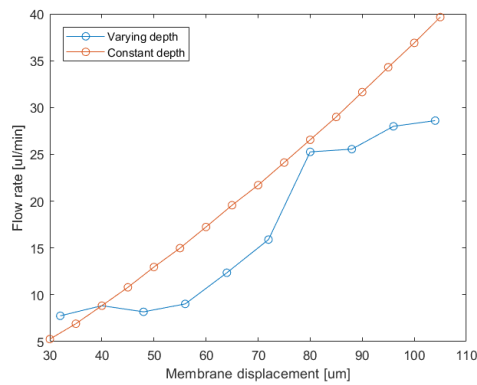


t	$\frac{18}{7}$ s	tt	tt
Δt	$\frac{1}{7}$ s	a	10°
f	3.5Hz	wn	150 µm
di	40 µm / 0.16tt	dd	1.5 mm
m	18 [mm]		

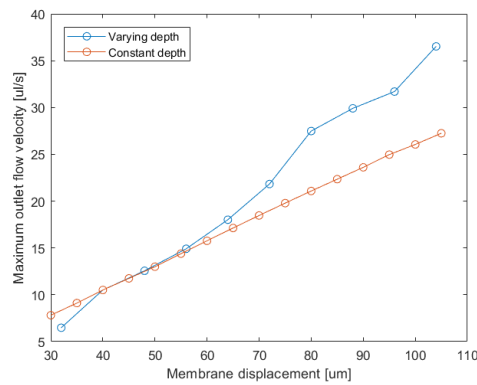
Figure 3.12: Flow rate output as a function of channel depth.

From inspection of the maximum outlet flow velocity for varying channel depth a steady trend is seen for the constant relative membrane displacement, while it hardly changes for the constant absolute displacement. This suggests that the channel depth has negligible influence on the flow pulses.

It must be noted that, when comparing the higher depth region to figure 3.9, it seems as if the higher flow rate for this region can be attributed almost exclusively to the larger membrane deflection. These two are compared below (figure 3.13). (Note that a new *di*-dataset was made to account for the adjusted membrane size.)



(a) Flow rate development



(b) Maximum outlet flow development

Figure 3.13: Membrane displacement for variable and constant channel depth

These plots show the results of two simulations: one with variable channel depth (but with constant displacement as a percentage of *tt*) and one with only a variable *di*.

Aside from a marginal difference at the low displacement range, in figure 3.13a can be seen that for the same displacement, the flow output is higher for a constant channel depth. In other words: *di* as a percentage of *tt* has significant influence. This can likely be attributed to the increased moved volume per stroke (relative to the chamber volume), as was explained in 1.4.3.

The opposite is true for the outlet flow pulse: if one aims to increase the amplitude of this pulse, increasing *tt* is more efficient than increasing *di* (as a percentage of *tt*), at least for membrane displacements above 65µm. This must be the effect of the larger pump chamber, with the increased volume allowing larger pulses for increasing *di*.

Concluding, it can be said that increased flow rate is most efficiently reached by increasing membrane displacement. For increased flow pulses this is achieved by increasing channel depth (but not relative displacement).

These have been the chamber parameters: the third and final parameter group is the nozzle parameters.

3.3.6. Nozzle angle

First of the nozzle parameters is the angle. The resulting flow rate development is given in figure 3.14.

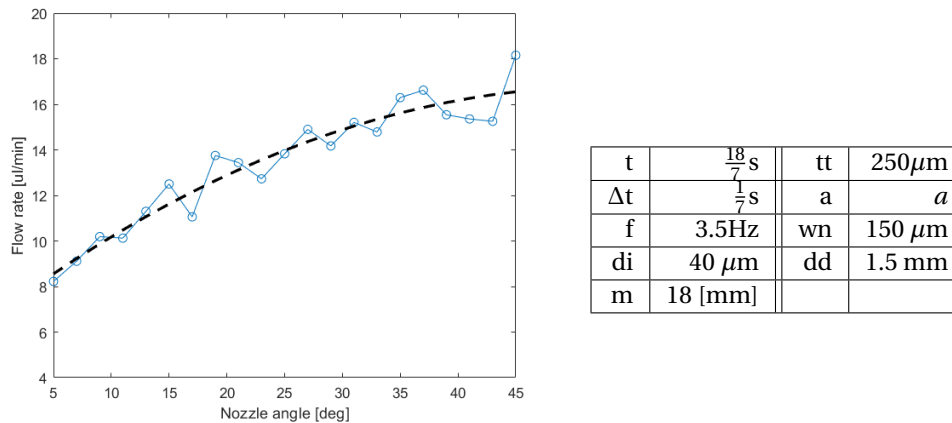


Figure 3.14: Flow rate output as a function of nozzle angle.

This flow rate development is not as smooth as previous ones, however, a parabolic fit is still made. This supports the intuitive notion that a wider angle increases the flow due to the decreased resistance, up to a certain degree. In 1.4.3 it was shown that the pump action depends on this resistive elements, although the beneficial effect has a maximum. Since the increasing effect is showing mostly at the smaller angles, the nozzle angle size is now increased to 20° in the model, again to make differences more pronounced. Concerning the outflow velocity, this shows little difference (see figure B.4a), both in amplitude and pulse frequency.

3.3.7. Nozzle width

This development too shows a parabolic fit to the dataset. Although the first few results in the parameter set are low, possibly because the resistance of the small opening is too high, a strong development is seen from about 90 μ m. This positive effect of reduced resistance flattens out as well, similarly to what was seen in the nozzle angle study.

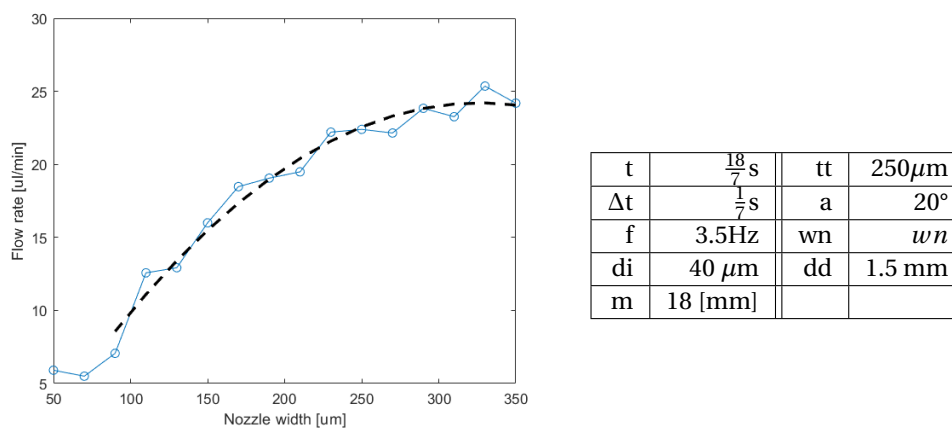


Figure 3.15: Flow rate output as a function of nozzle throat width.

Similarly to the nozzle angle study, the outlet flow seems independent of nozzle throat width (see figure B.5).

The findings of this study are not very consistent with those of for example Singh et al. [32]. who attribute their drop in flow rate output to choking of the nozzle. The author sees this as highly unlikely as that would mean flow reaches near-sonic (transient) conditions which is not very likely to happen in a microfluidic device. The

maximum seen here implies that at a certain point the nozzle effect becomes smaller due to its width, and this is then seen sooner at the high frequency that Singh et al use.

3.3.8. Nozzle length

The flow rate development of this sweep is seen in figure 3.16.

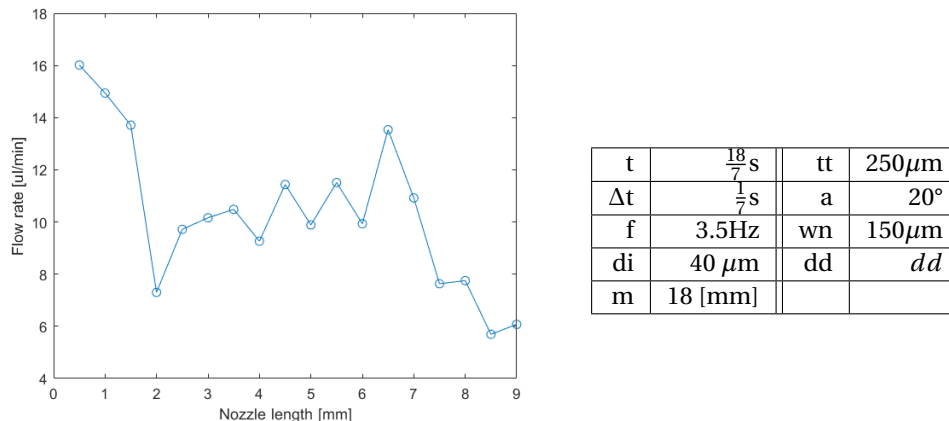


Figure 3.16: Flow rate output as a function of nozzle length.

This is the first parameter for which a decline (although not a consistent one) can be seen with an increase of parameter size. There is a region (between 2 and 6 mm) where the flow rate varies around 10 μ l/min, but after this the decline continues.

One of the only studies addressing this clearly is Singh et al. [32]. The peak they show is not present in this simulation, although it does decline above $dd=1$ mm. It must be noted that they only tested a very small range. The declining flow rate can be attributed to the increased pressure drop over the nozzle, which becomes significant from $dd=7.5$ mm onward.

The outlet flow velocity is not affected by the change in nozzle length (see figure B.4b).

3.4. Intermediate conclusions

When keeping the requirements for the three intended designs in mind, a number of conclusions can already be drawn from the past results.

1. There is a strong positive correlation between membrane frequency and displacement and flow rate output.
2. For membrane width a maximum range can be observed for flow rate output and maximum pulses.
3. Channel depth affects mostly the flow rate output but mostly the flow pulses.
4. Nozzle angle and width have a positive correlation with flow rate output (up to a maximum).
5. Nozzle length has a slightly negative correlation, most pronounced at small and large values.
6. None of the nozzle parameter sweeps has shown influence on the outlet flow pulses.
7. Most importantly: the values found in these simulations are not (always) consistent with literature and this suggests that a puzzle such as this one with many variables also has many solutions

Based on these conclusions, some hypotheses are formulated for the interaction study.

1. A positive correlation between a frequency-displacement sweep and flow rate / outflow velocity
2. A positive correlation between a membrane-channel depth sweep and flow rate, a very mild positive correlation for the same sweep and outflow velocity
3. A positive correlation between a nozzle width-nozzle angle sweep and flow rate
4. A very mild positive correlation between a nozzle width-nozzle length sweep and flow rate
5. A very mild positive correlation between a nozzle angle-nozzle length sweep and flow rate
6. No correlation for any nozzle parameters and outlet flow velocity
7. A very pronounced positive correlation between nozzle width and membrane displacement

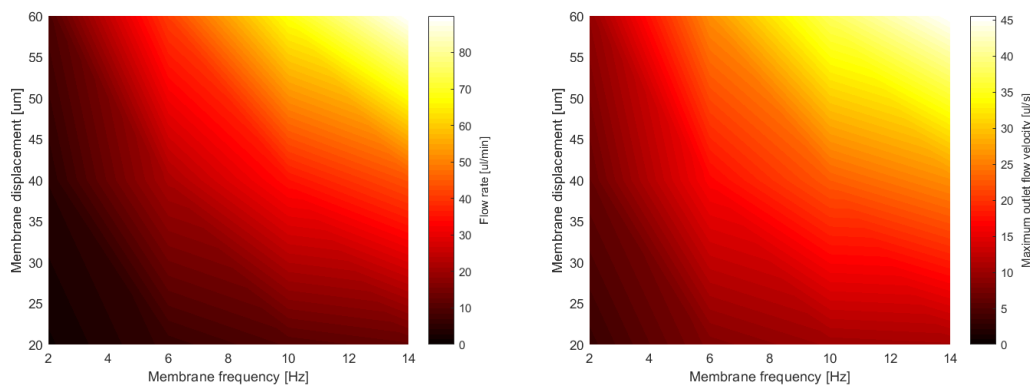
Based on all of these studies the optima are formulated.

3.5. Interaction characterization (results)

Six interaction studies were performed based on the intermediate conclusions drawn and hypotheses set in the previous section. As to perform the entire parameter sweep for all values would be computationally expensive and counterproductive, only selected values are studied in a range / interval which have shown to be interesting in the previous simulation. Note that in this part no parameter values are changed in the base model.

3.5.1. Membrane frequency-displacement correlation

An important interaction study is the frequency-displacement interaction. These are both parameters that remain variable after fabrication to a certain extent.



(a) Flow rate development as a function of membrane frequency and displacement

(b) Maximum outlet flow development as a function of membrane frequency and displacement

Figure 3.17: Membrane frequency - displacement interaction

The interaction follows a trend that could be expected from 3.3.2 and 3.3.3. Here too it can be seen that the effect is more pronounced for the membrane frequency. Overall, for higher f and di the efficiency becomes higher too: for a doubling pulse amplitude the flow rate triples.

This confirms that high membrane frequencies and high membrane displacements yield both high flow rates and high flow pulses. It must be noted here that the maximum possible displacement is limited by the membrane size and for a deeper channel depth, a larger displacement is needed to have the same effect (see figure 3.13).

3.5.2. Channel depth-membrane width correlation

Below the flow rate and maximum outlet velocity interactions are studied (figures 3.18, 3.19). Although larger membrane sizes were attempted for simulation, the simulation time increases exponentially from around 20mm and it was therefore not realistic to include them. This was likely due to a meshing issue that could not be resolved.

Note that the test in 3.3.5 showed that the membrane displacement should be treated as a percentage of the channel depth to see development of the flow rate, which was done here as well.

The correlation between these two is remarkably similar compared to their independent simulations: the development varies more or less linearly for the channel depth, and a maximum area is seen between 18-22mm membrane diameter. What can be seen as well (similarly to the simulation in 3.3.5) is a steep part for larger membrane sizes when looking at varying channel depth. It gets smoother when the membrane size gets larger.

In figures 3.20 and 3.21, data is plotted against the chamber volume. At larger chamber volumes a special development is seen: for the same volume, a higher efficiency and flow rate are reached when the channel width is smaller. This effect is seen above a volume of around 75 mm^3 . In 3.3.5 the effects of channel depth were already seen. However, this is limited by the maximum wafer thickness, therefore this advantage is limited too. For larger membrane sizes, however, the potential flow rate (and maximum outlet flow) becomes

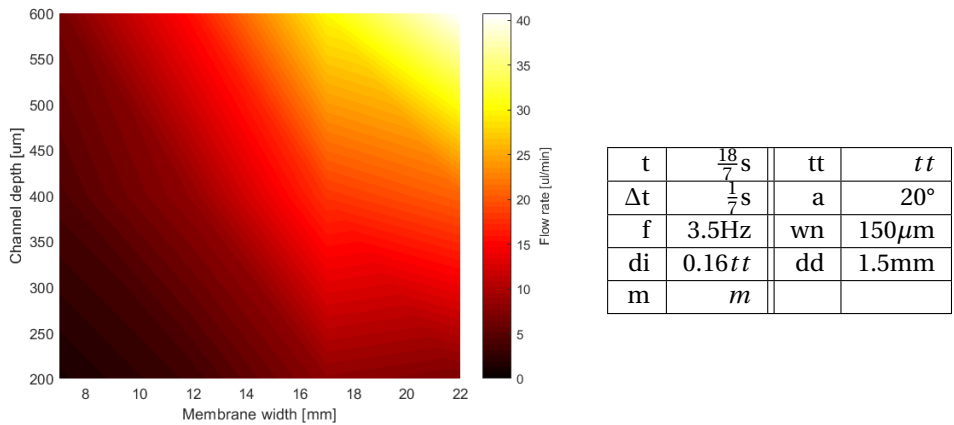


Figure 3.18: Flow rate development as a function of membrane width and channel depth

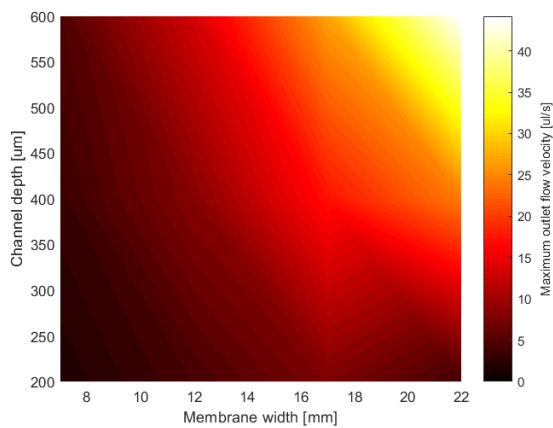


Figure 3.19: Maximum outlet flow development as a function of membrane width and channel depth

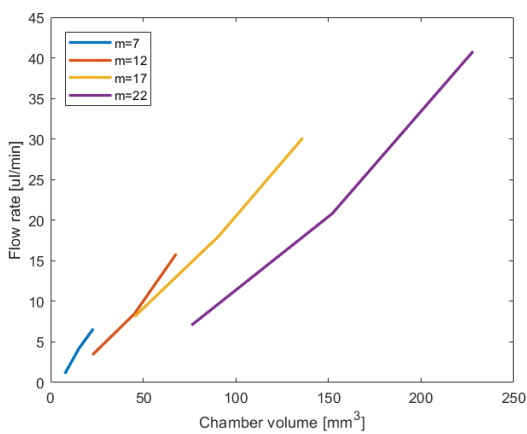


Figure 3.20: Flow rate as a function of chamber volume

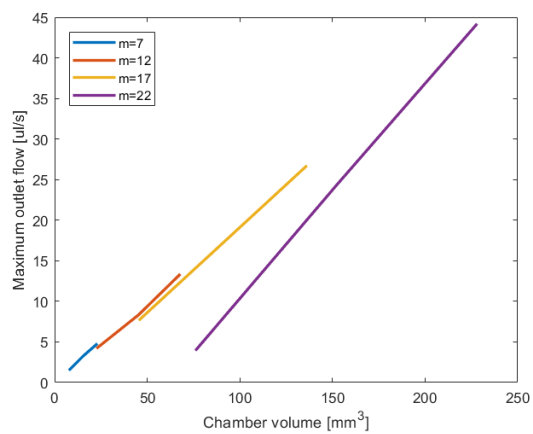


Figure 3.21: Maximum outlet flow as a function of chamber volume

higher too. This is in line with previous findings: the increased chamber volume increases the potential (much like a capacitor), with channel depth being the most prominent factor.

3.5.3. Nozzle parameter correlation

The interaction studies of the nozzle parameters are treated under this subsection together. First the nozzle width and angle are studied (see figure 3.22).

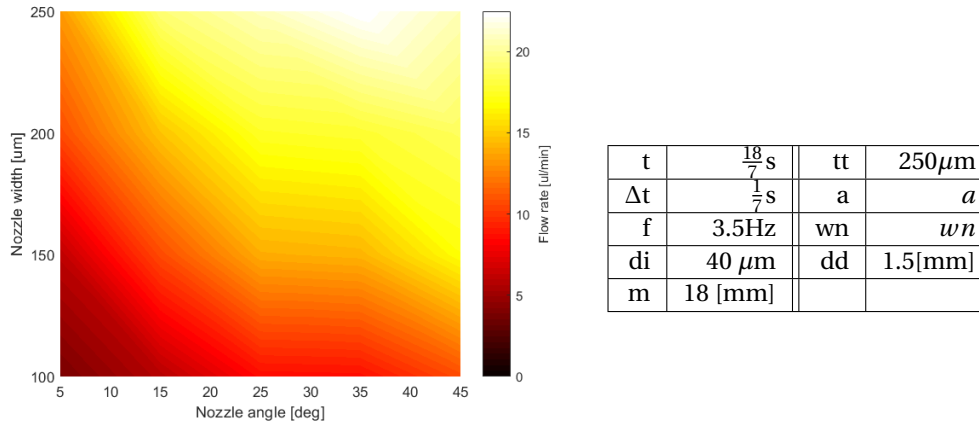


Figure 3.22: Flow rate development as a function of nozzle throat width and nozzle angle

The selected range for wn was based on the region where the maximum showed in 3.3.7. What stands out is that the increasing flow development reaches a maximum around 40°. This is most pronounced in larger nozzle widths: possibly in such large nozzles the effectiveness of the nozzle resistance reduces.

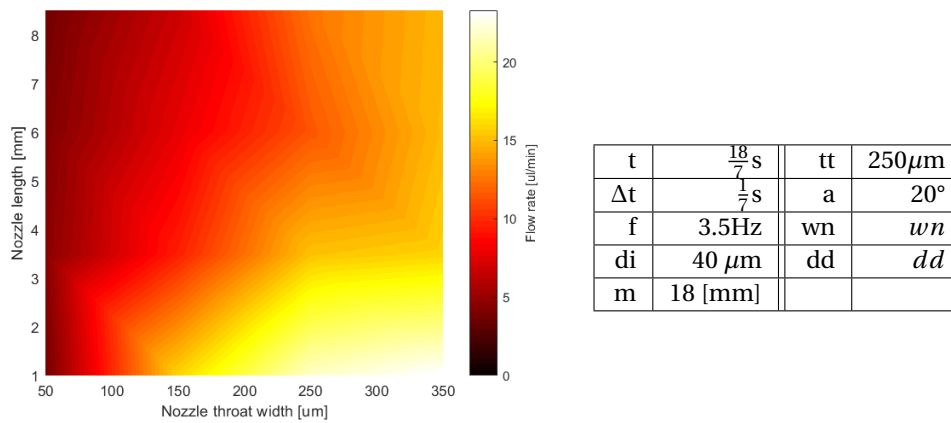


Figure 3.23: Flow rate development as a function of nozzle throat width and nozzle length

Following is the interaction between nozzle length and nozzle throat width (figure 3.23). Similarly to the single parameter study, the inverse relation between nozzle length and flow rate output is observed here, as well as the steep increase in output for very short nozzles. The increase in flow rate for varying wn is mostly seen at this short nozzle length whereas it becomes more gentle for longer nozzles.

Finally nozzle length and nozzle angle are compared (figure 3.24). The slope seen here is not as steep as with the changing nozzle throat width, however, it also leads to an ultimately lower flow rate than in the former two comparative simulations.

At the same time, it can be concluded that next to increasing nozzle throat width, increasing the nozzle angle is an effective way of increasing flow rate, even for longer nozzles.

One must note that these two parameters affect the width of the diverging side of the nozzle (wd) most effectively. It might be concluded that having a wd -value that approaches m yields a relatively good output increase - but not so much as having a shorter nozzle.

By theory from 1.4.3, the pump action generated by the nozzle was found to be most dependent on the resistance in the nozzle. (See figures 1.7a and 1.7b.) In order to have pump action a net flow from left to right

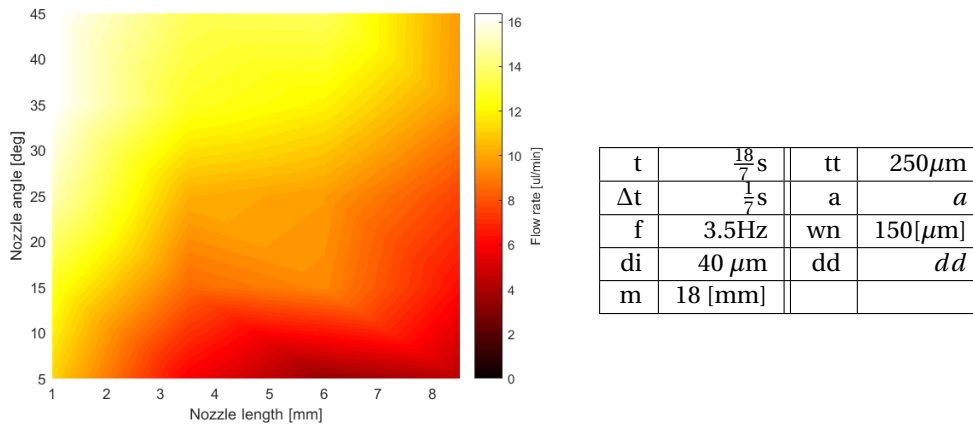


Figure 3.24: Flow rate development as a function of nozzle angle and nozzle length

is needed, meaning that over a nozzle the resistance from left to right must be low, from right to left it must be high. This can be described in terms of the findings of the nozzle parameter studies:

1. Nozzle throat width decreases resistance in left-to-right flow
2. Of the three parameters, this is the most critical one for efficient increase of pump output
3. Nozzle angle increases resistance from right to left, increasing pump effectivity in this way.

3.5.4. Nozzle width-membrane displacement correlation

The nozzle throat width was concluded to be the most influential dimension in terms of nozzle resistance. Moreover, in 1.4.3 it was concluded that membrane movement and nozzle resistance are critical in pump action efficiency, these two are studied together as well (see figure (3.25)). Similar parameter ranges were chosen as in previous studies.

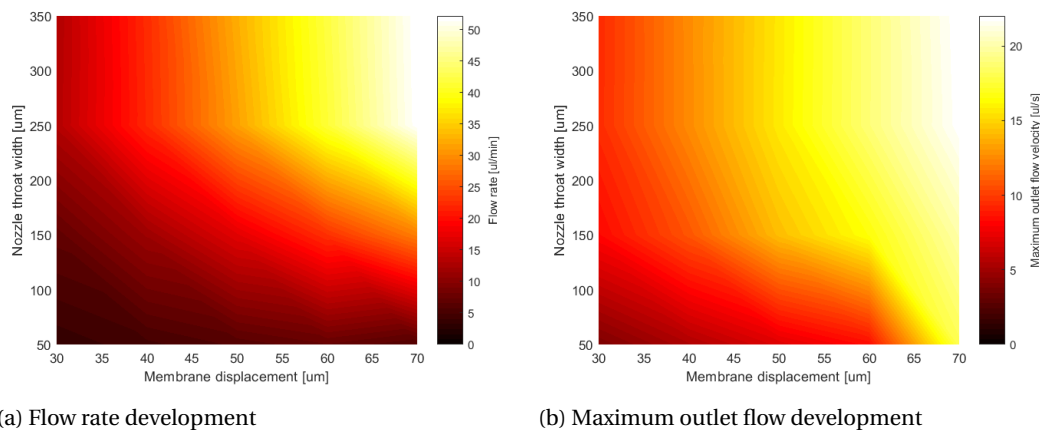


Figure 3.25: Nozzle throat width - membrane displacement interaction

This shows that the membrane displacement is one of the more significant factors in terms of flow output. However, it is also seen that the larger nozzle widths have their share in larger flow rates as well, even for very small membrane displacements.

The effect on outflow pulsing is evident as well. Although large flow pulses are unavoidable at large membrane displacements, they are kept at bay largely for very small nozzle throat widths (50-100 μm). Above this they remain more or less constant: this is likely caused by the relative small difference between intermediate values.

3.6. Alternative configuration results

Most studies in literature developed a single chamber / double nozzle configuration. Other configurations might still outperform them in terms of flow rate and outflow pulsing (compared to the basic configuration). A number of alternative models have been tested by Ullman [35]. Another model is tested here, being a double-nozzle configuration: it has two nozzles up- and downstream of the pump chamber (see figure 3.26). As the figure shows, the nozzles have been "exaggerated" to make any effects show up clearly: all nozzle parameters have been set to their maximum mode (large wn and a and small d).

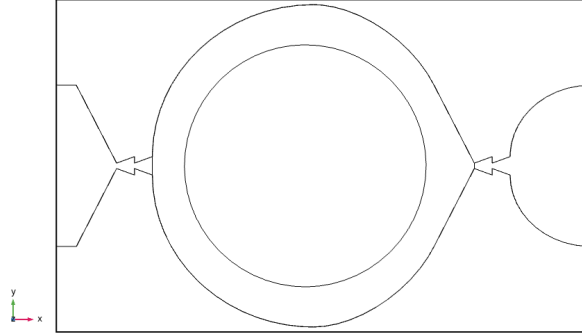


Figure 3.26: Top view of the double-nozzle configuration

In figure 3.27 the effect of the double nozzle can be viewed. It does not have much effect: the flow rate is calculated to be 8.83 and 5.36 $\mu\text{l}/\text{min}$ for the single- and double nozzle configuration respectively. For the outflow pulses, little difference can be spotted. A more extensive study is possibly able to express larger differences (for example at larger f and d_i) but this is beyond the scope of this project.

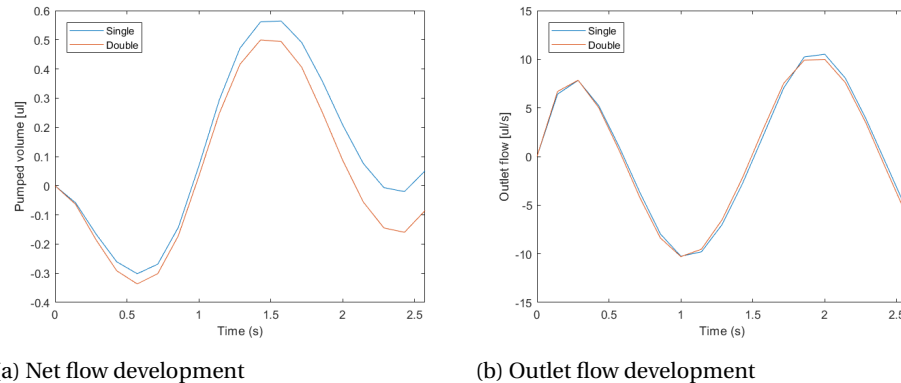


Figure 3.27: Comparison between the single- and double nozzle configuration.

3.7. Conclusion

This chapter carried out the simulations needed to come to the designs set in chapter 1 using the model made in chapter 2. First a verification step determined the membrane eigenfrequency and confirmed laminar flow. The simulations were carried out by first studying parameters independently and after this interaction studies were performed as well. The theory from 1.4.3 was seen in that membrane displacement/movement and nozzle resistance have important roles in terms of flow output. However, many optimal values found in literature were not. This can likely be attributed to the large difference in membrane frequency, which was the most significant of all variations with literature. It is then evident that for a lower-frequency device other dimensions are fitting. Although theory could provide sensible explanations for most phenomenae, this was not always the case for literary background. It does not mean others were wrong, it does show that a puzzle such as this with many variables has many solutions. Those presented in this thesis are but three of possibly many more. The findings from this chapter have been combined in three model propositions as suggested in 1.4.4 and are analyzed in chapter 4.

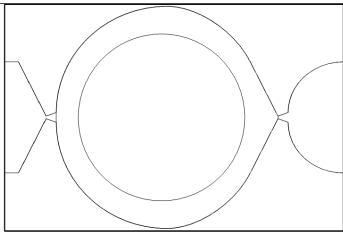
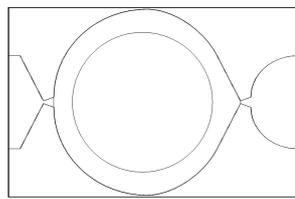
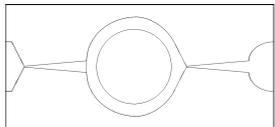
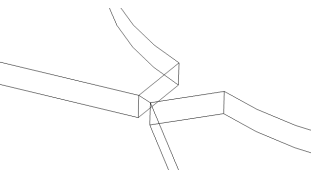
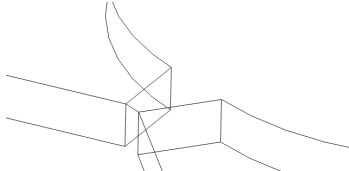
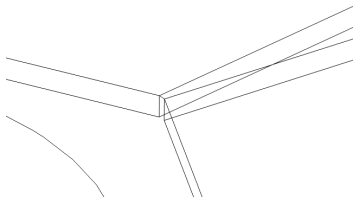
4

Results

In this chapter the design options are laid out and justified. For each design the specifications are explained, shown, and a number of simulations are done to confirm the expected model properties. First the three designs are compared (section 4.1). The design options are a high flow rate model (section 4.2), a high flow pulse model (section 4.3) and the low flow rate and pulse model (section 4.4), all of which are characterized. A summary is given in the conclusion (section 4.5).

4.1. Design overview

Below the three design choices are depicted. They are elaborated upon in their respective sections.

	High flow rate	High flow pulse	Low flow rate / pulse
Top view			
Nozzle close-up			
m	22 mm	18 mm	12 mm
tt	350 μm	600 μm	300 μm
wn	250 μm	250 μm	100 μm
a	40°	40°	10°
dd	1 mm	1 mm	7.5mm

4.2. High flow rate design

The first design concerns the model aimed at OoC applications that require high flow rate, for example liver and tumor models (see 1.2 and 1.4.4) The dimensions were based on the following findings:

- Large membrane displacement yield higher flow rates: the large membrane width means there is a larger maximum di possible.
- The channel depth is kept slightly deeper than the maximum possible displacement, since a higher percentual displacement is shown to have a positive effect on flow rate.

- The nozzle are short and wide, allowing easy flow in flow direction and more resistance in backflow direction.

This yields the following model specifications:

Dimensions			
m	22mm	a	40 °
tt	350 μm	wn	250 μm
di _{max} ^a	295 μm	dd	1mm

Table 4.1: "High flow rate" design properties overview

^aTheoretical maximum

The top view of the model can be viewed in figure 4.1.

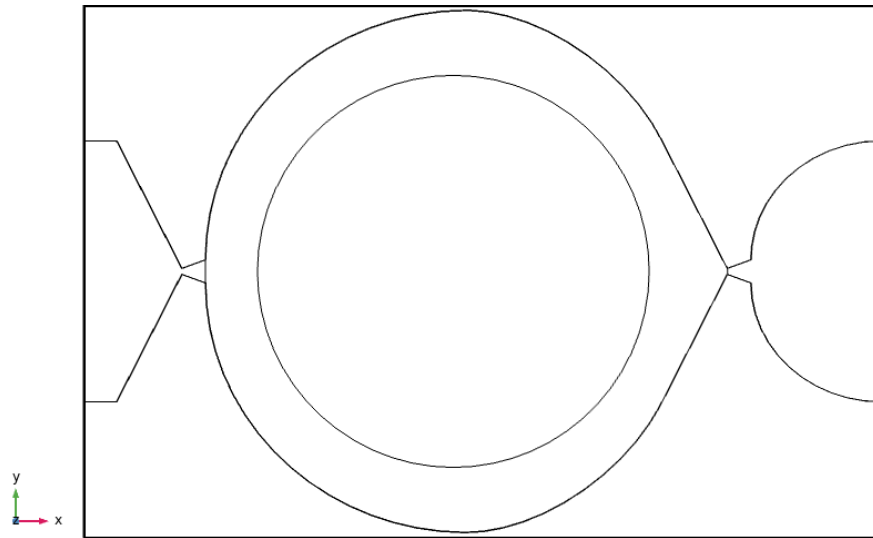
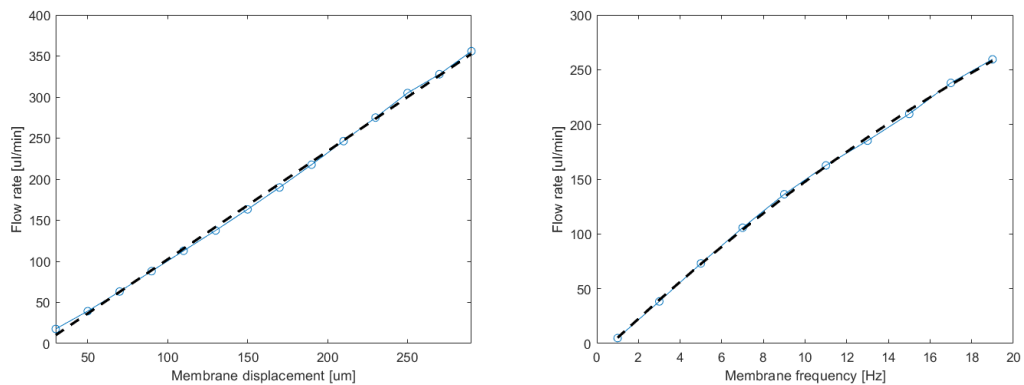


Figure 4.1: Top view of "high flow rate" design

The model is tested in parameter sweeps for membrane displacement and membrane frequency (see figure 4.2). In order to be able to study a large range of values, no interaction study was performed to avoid many errors and long simulation times.



(a) Flow rate for varying membrane displacement (f=3.5Hz)
(b) Flow rate for varying membrane frequency (di=56 μm)

Figure 4.2: Membrane frequency and displacement flow rate development for the "high flow rate" design

The flow rate outputs for variable membrane displacement (figure 4.2a) and membrane frequency (figure 4.2b) are given. The flow rate shows a large potential compared to the base model: up to $350 \mu\text{l}/\text{min}$ for maximum displacement and up to $250 \mu\text{l}/\text{min}$ for the maximum tested frequency. The flow is also very efficient compared to the outlet flow pulses (see figure B.6a and B.6b): while the flow rate normally is in the same range as the outflow pulses, for this design the pulses are relatively small, about a third of the value of the flow rate output. This confirms the theory that a medium shallow channel and the current nozzle configuration yields a smoother (and thus efficient) flow. It also shows once again that membrane displacement is a more effective way of increasing flow output than membrane frequency. However, as the former is likely limited due to material constraints, the option of an increased frequency should be kept in mind as well.

4.3. High pulsing design

This design is meant for OoC applications that require a more pulsing flow behavior, for example for atherosclerosis models or the heart. It means that the flow velocity has a high fluctuation amplitude (specifically in relation to the flow rate). The model characteristics came to this based on the following findings:

- Since a high flow pulse and high flow rate are inherently connected, this design and the previous one are similar in some ways.
- The most important difference is seen in the size and shape of the pump chamber, which has a more "square" intersection. The membrane diameter was chosen based on the maximum found in 3.3.4 whereas the channel is rather deep, as this is more effective for pulse increment (see figure 3.13b).
- In order to make this model more realistic, it should be operated in such a range that outflow pulses are between 1-1.6 Hz or at resting heart rate.

This yields the design characteristics described in table 4.2.

Dimensions			
m	18mm	a	40°
tt	$600 \mu\text{m}$	wn	$250 \mu\text{m}$
di_{max}^a	$142 \mu\text{m}$	dd	1mm

Table 4.2: "High pulsing" design properties overview

^aTheoretical maximum

The resulting design top view can be viewed in figure 4.3.

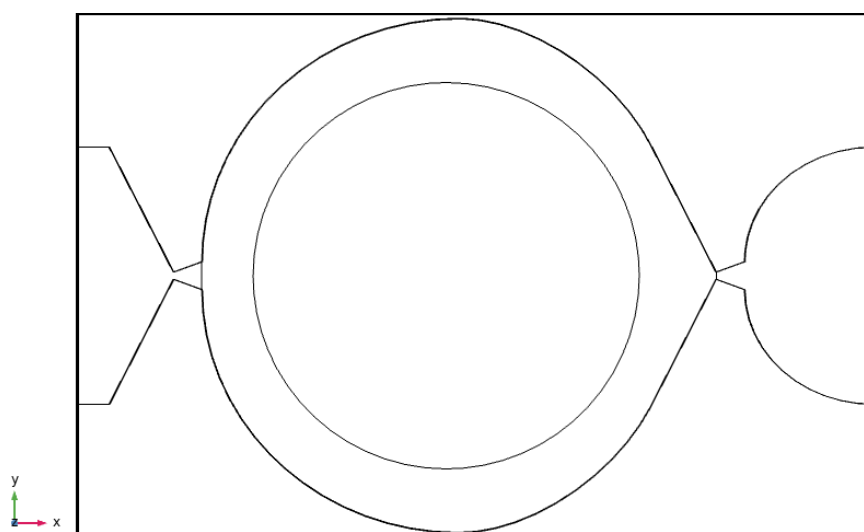


Figure 4.3: Top view of "high pulsing" design. Note that the nozzle shapes are the same for this model as the previous one, only the membrane diameter and channel depth have changed.

For a comparison to the "high flow rate" design this model is tested for both flow rate and outflow pulse for membrane displacement and a range of frequencies that are in "heart rate range". Keeping in mind the conversion discussed in 3.3.2, for heart rates of 60-100 bpm this translates to membrane frequencies of 6 to 10 Hz.

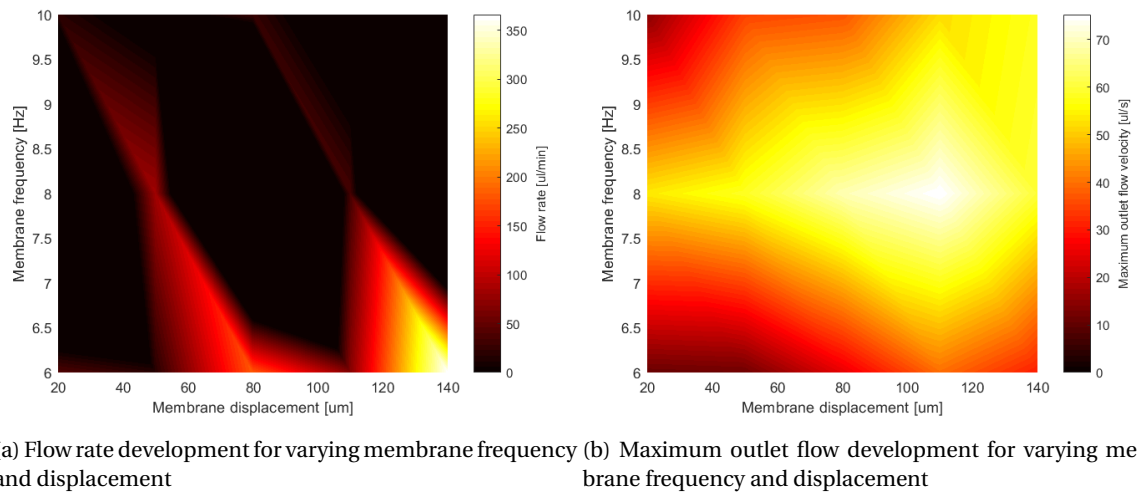


Figure 4.4: Membrane frequency-displacement interaction for "high pulsing" design

What stands out is that the flow rate development does not seem continuous. Possibly this can be attributed to the size of the dataset (as the range of possible membrane displacements is very limited). For most of the dataset the resulting flow rate is on the low side, except for a small area for high di . The outlet flow is different. Compared to the "high flow rate" dataset, this design performs only slightly better in terms of outlet flow pulses. However, it must be noted that in almost all cases a high flow rate is accompanied by a high outlet pulse in absolute sense: here the relation to the flow rate is more interesting. This shows that it is indeed possible to have a strong flow pulse without a very high flow rate, if one stays clear of the combination high flow rate and low frequency. What stands out is that optimal conditions are not reached only at the maximum membrane displacement. This is positive, as it is not certain this deflection is actually possible in a real-life situation: this shows that a deflection of 100-120 μm is sufficient in this design.

4.4. Low flow rate and pulsing design

The last model is one meant for situations where fine-tuning of very low flow rates and pulses is desired: the lungs are exemplary of this, but another application might be models of neonatal organs. The findings related to this design are the following:

- The membrane diameter is small enough that the flow output is low but that the maximum membrane displacement is still large enough to be able to vary it somewhat.
- The lower tt value ensures that the relative displacement is low and the chamber volume is small.
- While the short and squat nozzles from the previous two designs yield larger flow outputs, these are more slender.

The following characteristics were set for this design:

Dimensions			
m	12mm	a	10°
tt	300 μm	wn	100 μm
di_{max}^a	42 μm	dd	7.5mm

Table 4.3: "Low flow rate and pulsing" design properties overview

^aTheoretical maximum

The top view of this configuration can be found in figure 4.5,

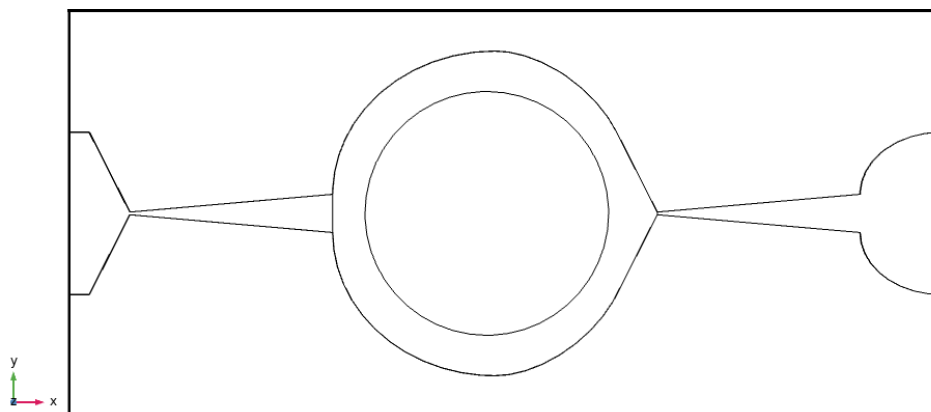
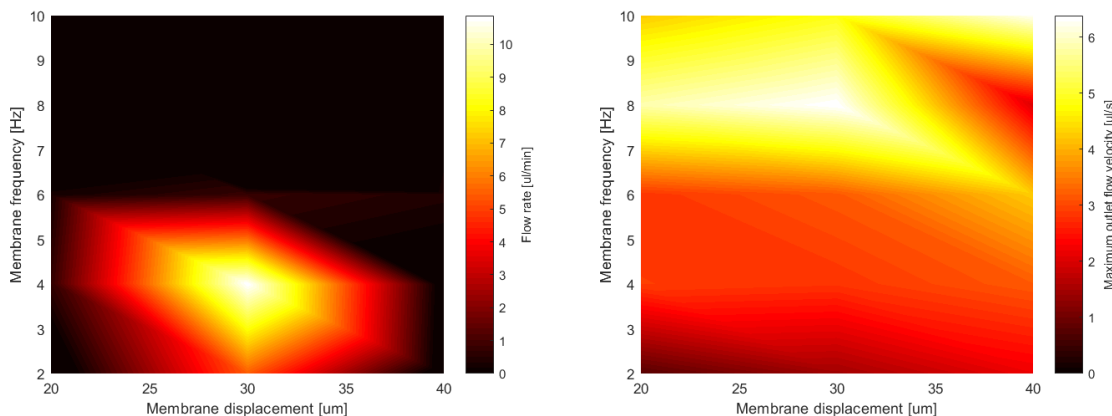


Figure 4.5: Top view of "low flow rate and pulsing" design

The simulation for this model is a short one, since the range of membrane displacements is small as the maximum theoretical displacement is only 42μ . The results can be reviewed in figure 4.6.



(a) Flow rate development for varying membrane frequency and displacement (b) Maximum outlet flow development for varying membrane frequency and displacement

Figure 4.6: Membrane frequency-displacement interaction for "low flow rate and pulsing" design

This confirms the low flow rate and low flow pulses. In the higher flow rate range (frequencies between 2 and 6 Hz and membrane movements between 25 and 35 μm) the pulses are low as well. The reverse is true when looking at the other half tested f values. An explanation for this would be that in the first case, energy is used to generate pump action, whereas for higher frequencies that energy only serves to pulse the flow back and forth. Possibly the higher membrane frequency overcomes the resistance the nozzle should provide to the backflow, omitting pump action, whereas the lower frequencies have too little energy for this. An operating range of a frequency between 2 and 6 Hz and membrane displacement between 25 and 35 μm is recommended for this model. It must be noted, though, that previous simulations showed slightly irregular results for the low membrane frequency-displacement range: a larger simulation study is recommended to confirm this behavior.

4.5. Conclusion

Three models were set up according to the findings in chapter 3 and simulated to verify their effectivity.

All models were consistent with the findings found in previous simulations. The high flow rate model has efficient strokes thus providing a high output. The high flow pulse model likely has room for improvement: although the pulse in relation to the flow rate is high, dimensional parameters could still be tweaked to see higher pulses. The low flow rate/ pulse model indeed shows low flow rates, however, it is known that small membrane movement results might behave irregularly. It must be noted, that although these designs provide a good result for their intended purpose, there are endless possible configurations and this is by no means the only way to obtain these results.

The fabrication and actual testing of these models are beyond the scope of this project, but recommendations for these processes are given in chapter 5.

5

Recommendations

Not all aspects of a full pump design - from initial research to testing and implementation - could be incorporated in this thesis. Neither could all imperfections be erased and corrected for the design process. For this reason, a number of recommendations for (a) future project(s) are laid out in this chapter, with the intention of providing others with suggestions for continuation.

Recommendations for improvement of the past project are discussed for modelling and simulations (section 5.1). For continuation, suggestions are given for fabrication (section 5.2) and testing (section 5.3). These are summarized in the conclusion (section 5.4).

5.1. Modelling and simulation improvements

Some discussion points were already mentioned in section 2.6. These and others are listed below.

1. The membrane model is rather simple in this design. If one would aspire a more reliable result, some things could be implemented:
 - (i) The actual materials are implemented as well as the real-life deformation, rather than a moving disc
 - (ii) The movement can take place based on applied force or even voltage (including the physics involved) instead of the current prescribed displacement. Obviously, the latter would be much more complex and require a thorough understanding of the physics involved.

This might raise (and answer) the following questions:

- (a) How does the presence of a PDMS membrane affect the movement of the IPMC? Are there better ways to construct this in the model?
- (b) How does the PDMS thickness relate to the membrane movement and pump efficiency? What is the minimum thickness that allows unhindered movement but is stiff enough to avoid failure?
- (c) How well does the membrane perform over a longer time? Does the behavior change over time, does the material fatigue, and if so, how?

All of these effects likely need to be verified through testing, but they can be better predicted if these aspects are implemented first.

2. The design can be improved by eliminating the excess material on the sides of the channel and replacing it with a boundary only. The excess material is not providing any meaningful solutions at the moment while taking up computational effort and power. If someone were to recreate the model rather than using this one, this should definitely be taken into account.
3. Although a resolution has been found to greatly reduce the number of errors for which no solution is returned, it would be better to try and see if there are other ways to mitigate this, as the Jacobian update adjustment is very computationally expensive.
4. Unfortunately during the project it became clear that in this model it is not always possible to extract the results from the channel midline velocities. Especially in the nozzle parameters, the nozzle velocity behavior would provide interesting insights in their influence on the flow. Although the results did generate well in COMSOL, exporting them for further processing was not possible due to a meshing error, and possibilities to generate comparative plots with useful results are limited without exporting

the data. The solution here would either be to solve the meshing issue or finding ways to process the relevant information in the software anyway.

5. When implementing the design in an OoC device, the model could be extended to include, for example, an open well with an irregular membrane one the side, representing a cultured tissue membrane. This is more similar to the proposed testing setup in section 5.3.
6. The device can be tested to include possibilities for application with gaseous substances as well.
7. To improve performance, there are passive methods available for microfluidic pumping that might help, such as hydrophobic strips along the channel [9]
8. There are many efficiency steps that can still be taken in the data postprocessing. The MATLAB scripts are by no means perfect and can still be improved to reduce manual effort even more:
 - (a) COMSOL tends to generate the data in a slightly unpredictable format: not all options for output are always available (such as having the parameters for columns rather than one parameter column). To recognize different data files better can improve the postprocessing routine.
 - (b) Currently some lines in the datafile need to be removed manually: this can likely be automated as well.
 - (c) Automatic generation of plot files and legends would also greatly reduce postprocessing effort.

Although the current model works well when properly acquainted with it, to make it more user-friendly and generally usable these steps will make sure someone unfamiliar can extract meaningful data from this model with minimum effort.

5.2. Fabrication

Fabrication has been an intended part of this project but as the process evolved was omitted from the final requirements. This section serves as a fabrication suggestion for a continuation of this project. Some sketches were made of the proposed testing models (see appendix D) using Autodesk Fusion 360 CAD software. The model includes an area that might be used for direct cell culturing or a platform such as Cytostretch [12]. Below a global process is written out. This is a process based on the intermediate solution of a PDMS membrane instead of the IPMC.

1. Use wafers with thickness such that the channel depth can be etched out.
2. The microfluidic circuits are manufactured using standard lithography and DRIE processes
3. For the PDMS membrane, a separate set of carrier wafers are silanized (to increase hydrophobicity)
4. PDMS is spin coated on top
5. The PDMS can now be attached to the wafer containing the microfluidic circuits using oxygen plasma activation, after which the carrier wafer can be removed
6. The devices can now be diced for testing

Note that there is an option to vary the channel depth to make a more varied testing spectrum. Again, this method is describing a fabrication method using an intermediate solution with a PDMS membrane instead of the IPMC configuration. If the latter is already fit to be implemented yet, this also requires design of integration aspects such as the circuitry, which is beyond the scope of this project. Furthermore, one might experiment with a semicircular channel outside of the nozzle-diffuser and pump chamber area to make postprocessing calculations more easy when testing.

5.3. Testing

Although the testing method is highly depending on the final choice of device configuration, a testing method is suggested here. This again assumes the PDMS membrane setup.

We test to verify the simulations and to determine its reliability. The most important questions to be answered are the following:

1. Is the flow rate development similar to the flow rate of the model?
2. Is the pulsing behavior the similar to the behavior of the model?
3. If not, in what way does it differ and how can this be explained?
4. Are there any other significant issues that arise during a practice test which have not been taken into account previously?

These questions should be answered using a test setup using the following items.

1. An actuation device to move the membrane. Some options are available for this.
 - (a) A mechanical actuation system, using a linear actuator attached to the membrane. This is the simplest option which requires no conversion from the model, which is based on prescribed membrane displacement.
 - (b) A pneumatic actuation system, applying pressure on the membrane and consequently moving it. This requires conversion of the applied pressure (force) to a resulting membrane displacement.
 - (c) A electromagnetic actuation system. This is not recommended, as the displacement is hard to control, but it might be implemented as a preliminary proof-of-concept testing method if the above ones are not available.
2. The measurement of the flow rate can be calculated using a pressure probe, thin film pressure measurement (with a working principle very similar to strain gauges) or laser velocimetry, for example using the doppler shift in a laser beam to calculate the fluid movement.

By measuring the flow pressure, the local flow velocity can be calculated using $P_{tot} = p_{static} + p_{dyn}$ and $P_{dyn} = \frac{1}{2}\rho v^2$. Then assuming the flow has a parabolic shape, the flow rate can be estimated by taking the integral: the flow rate is equal to $v \cdot A$ (with A the channel area) and the average velocity is the integral divided by A . Furthermore, the momentary flow gives indication of the flow pulsing.

Some possible issues that might emerge during testing are listed below.

1. Bubble formation is addressed in most literature as a possible issue. This should be monitored carefully.
2. A too thin membrane might bulge during testing. This might be prevented by constraining it, applying a thicker membrane, using a stiffer PDMS or applying a smaller displacement
3. The probe placement and its dimensions relative to the channel must be taken into account when using its data to draw conclusions
4. Accuracy should be considered carefully both for the actuation and the pressure measurements considering the small scale and the errors this might cause

Using these guidelines will provide a good framework for the device test setup.

5.4. Conclusion

Due to time constraints not all steps from design to fabrication and testing could be executed. In this chapter, recommendations are given for continuation of the project. These concern improvements on the modelling and simulations (i.e. things that *were* treated in this project) and future continuation of actual fabrication, testing and possibly implementation.

6

Conclusion

The aim of this thesis has been to design an on-chip pumping mechanism for OoC devices to improve user friendliness and facilitate mass production implementation. This led to an IPMC membrane pump with a nozzle-diffuser channel to generate pump action as the basis. The advantage to this is that no moving parts are needed in the channel. IPMC is very suitable for OoC application due to its operation in low-current conditions as well as its biocompatibility.

A model of the design was made in COMSOL Multiphysics, with the intention of characterizing the model dimensions and their impact on the flow. This then led to three designs: one for high flow rate applications, one for high flow pulsing applications, and finally one for low flow rates and more continuous flow. All three models were consistent with the theoretical expectations, with the sidenote that a model for high flow rate will inevitably also generate high flow pulses (and vice versa): the model can be improved still if the flow rate can be lowered while keeping the pulses high.

Based on this thesis, it can be concluded that it is possible to make a very small scaled micropump with significant output, as well as a smaller sized device for lower output applications. The combination of nozzle diffuser and IPMC allows for a device that can be produced using wafer fabrication techniques and thus for potential widespread implementation.

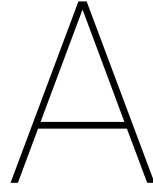
Bibliography

- [1] COMSOL Multiphysics 5.4, 2018.
- [2] Aysha Akhtar. The Flaws and Human Harms of Animal Experimentation. *Cambridge Quarterly of Healthcare Ethics*, 24(4):407–419, 10 2015. ISSN 14692147. doi: 10.1017/S0963180115000079. URL <http://www.ncbi.nlm.nih.gov/pubmed/26364776><http://www.pubmedcentral.nih.gov/articlerender.fcgi?artid=PMC4594046>.
- [3] Anthony K. Au, Hoyin Lai, Ben R. Utela, Albert Folch, Anthony K. Au, Hoyin Lai, Ben R. Utela, and Albert Folch. Microvalves and Micropumps for BioMEMS. *Micromachines*, 2(2):179–220, 5 2011. ISSN 2072-666X. doi: 10.3390/mi2020179. URL <http://www.mdpi.com/2072-666X/2/2/179>.
- [4] Yih Lin Cheng and Jiang Hong Lin. Manufacture of three-dimensional valveless micropump. *Journal of Materials Processing Technology*, 192-193:229–236, 2007. ISSN 09240136. doi: 10.1016/j.jmatprotec.2007.04.055.
- [5] Aerim Choe, Sang Keun Ha, Inwook Choi, Nakwon Choi, and Jong Hwan Sung. Microfluidic Gut-liver chip for reproducing the first pass metabolism. *Biomedical Microdevices*, 19(1), 2017. ISSN 15728781. doi: 10.1007/s10544-016-0143-2. URL <https://link.springer.com/content/pdf/10.1007%2Fs10544-016-0143-2.pdf>.
- [6] Genevieve Conant, Benjamin Fook Lun Lai, Rick Xing Ze Lu, Anastasia Korolj, Erika Yan Wang, and Milica Radisic. High-Content Assessment of Cardiac Function Using Heart-on-a-Chip Devices as Drug Screening Model. *Stem Cell Reviews and Reports*, 13(3):335–346, 2017. ISSN 15586804. doi: 10.1007/s12015-017-9736-2. URL <https://link.springer.com/content/pdf/10.1007%2Fs12015-017-9736-2.pdf>.
- [7] Andrew de Mello. Focus: Plastic fantastic? *Lab on a Chip*, 2(2):31N, 5 2002. ISSN 1473-0197. doi: 10.1039/b203828p. URL <http://xlink.rsc.org/?DOI=b203828p>.
- [8] Eva-Maria Dehne, Tobias Hasenberg, and Uwe Marx. The ascendance of microphysiological systems to solve the drug testing dilemma. *Future Science OA*, 3(2):FSO0185, 2017. doi: 10.4155/fsoa-2017-0002.
- [9] Ludivine C. Delon, Azadeh Nilghaz, Edward Cheah, Clive Prestidge, and Benjamin Thierry. Unlocking the Potential of Organ-on-Chip Models through Pumpless and Tubeless Microfluidics. *Advanced Healthcare Materials*, 1901784:1–9, 2020. ISSN 21922659. doi: 10.1002/adhm.201901784.
- [10] Denis Desmaële, Mehdi Boukallel, and Stéphane Régnier. Actuation means for the mechanical stimulation of living cells via microelectromechanical systems: A critical review. *Journal of Biomechanics*, 44(8): 1433–1446, 2011. ISSN 00219290. doi: 10.1016/j.jbiomech.2011.02.085.
- [11] Nobuyuki Futai, R. Paine, Shuichi Takayama, Hideki Fujioka, James B Grotberg, Y.-C. Tung, and Dongeun Huh. Acoustically detectable cellular-level lung injury induced by fluid mechanical stresses in microfluidic airway systems. *Proceedings of the National Academy of Sciences*, 104(48):18886–18891, 2007. ISSN 0027-8424. doi: 10.1073/pnas.0610868104. URL www.pnas.org/cgi/doi/10.1073/pnas.0610868104<http://www.pnas.org/cgi/doi/10.1073/pnas.0610868104>.
- [12] Nikolas Gaio, Berend van Meer, William Quirós Solano, Lambert Bergers, Anja van de Stolpe, Christine Mummery, Pasqualina M. Sarro, and Ronald Dekker. Cytostretch, an Organ-on-Chip platform. *Micromachines*, 7(7):1–14, 2016. ISSN 2072666X. doi: 10.3390/mi7070120.
- [13] Yaqiong Guo, Zhongyu Li, Wentao Su, Li Wang, Yujuan Zhu, and Jianhua Qin. A Biomimetic Human Gut-on-a-Chip for Modeling Drug Metabolism in Intestine. *Artificial Organs*, 42(12):1196–1205, 2018. ISSN 15251594. doi: 10.1111/aor.13163.

- [14] Sasan Jalili-Firoozinezhad, Francesca S Gazzaniga, Elizabeth L Calamari, Diogo M Camacho, Cicely W Fadel, Bret Nestor, Michael J Cronce, Alessio Tovaglieri, Oren Levy, Katherine E Gregory, David T Breault, Joaquim M. S Cabral, Dennis L Kasper, Richard Novak, and Donald E Ingber. Complex human gut microbiome cultured in anaerobic human intestine chips. *bioRxiv*, page 421404, 2018. doi: 10.1101/421404. URL <http://dx.doi.org/10.1101/421404><https://www.biorxiv.org/content/early/2018/09/20/421404?%3Fcollection=>.
- [15] Kyung Jin Jang, Ali Poyan Mehr, Geraldine A. Hamilton, Lori A. McPartlin, Seyoon Chung, Kahp Yang Suh, and Donald E. Ingber. Human kidney proximal tubule-on-a-chip for drug transport and nephrotoxicity assessment. *Integrative Biology (United Kingdom)*, 5(9):1119–1129, 8 2013. ISSN 17579694. doi: 10.1039/c3ib40049b. URL <http://xlink.rsc.org/?DOI=c3ib40049b>.
- [16] Andrew Evan Kamholz and Paul Yager. Molecular diffusive scaling laws in pressure-driven microfluidic channels: Deviation from one-dimensional Einstein approximations. *Sensors and Actuators, B: Chemical*, 82(1):117–121, 2002. ISSN 09254005. doi: 10.1016/S0925-4005(01)00990-X. URL https://ac.els-cdn.com/S092540050100990X/1-s2.0-S092540050100990X-main.pdf?_tid=aa10942d-f26b-46d0-9428-837eb8699daa&acdnat=1551388422_da34cf0afe57a7d8119912cd6cf20300.
- [17] Paul Kawun, Stephane Leahy, and Yongjun Lai. A thin PDMS nozzle/diffuser micropump for biomedical applications. *Sensors and Actuators, A: Physical*, 249:149–154, 10 2016. ISSN 09244247. doi: 10.1016/j.sna.2016.08.032.
- [18] Robert G. Mannino, Navaneeth K.R. Pandian, Abhishek Jain, and Wilbur A. Lam. Engineering “endothelialized” microfluidics for investigating vascular and hematologic processes using non-traditional fabrication techniques. *Current Opinion in Biomedical Engineering*, 5:13–20, 3 2017. ISSN 24684511. doi: 10.1016/j.cobme.2017.11.006. URL <https://linkinghub.elsevier.com/retrieve/pii/S2468451117300831>.
- [19] Elaine N. Marieb and Katja Hoehn. *Human anatomy & physiology*. Pearson, 10th edition, 2016.
- [20] Ilka Maschmeyer, Alexandra K Lorenz, Katharina Schimek, Tobias Hasenberg, Anja P Ramme, Juliane Hübner, Marcus Lindner, Christopher Drewell, Sophie Bauer, Alexander Thomas, Naomia Sisol Sambo, Frank Sonntag, Roland Lauster, and Uwe Marx. A four-organ-chip for interconnected long-term co-culture of human intestine, liver, skin and kidney equivalents. *Lab on a Chip*, 15(12):2688–2699, 2015. ISSN 14730189. doi: 10.1039/c5lc00392j. URL www.rsc.org/loc.
- [21] Anurag Mathur, Peter Loskill, Kaifeng Shao, Nathaniel Huebsch, Soon Gweon Hong, Sivan G. Marcus, Natalie Marks, Mohammad Mandegar, Bruce R. Conklin, Luke P. Lee, and Kevin E. Healy. Human iPSC-based cardiac microphysiological system for drug screening applications. *Scientific Reports*, 5(1):8883, 8 2015. ISSN 20452322. doi: 10.1038/srep08883. URL <http://www.nature.com/articles/srep08883>.
- [22] T.H.G. Megson. *Aircraft structures for engineering students*. Elsevier, 4th edition, 2007.
- [23] Paul Motreuil-ragot, Andres Hunt, Dhanesh Kasi, Bruno Brajon, Arn Van Den Maagdenberg, Valeria Orlova, Massimo Mastrangeli, and Pasqualina M Sarro. Enabling actuation and sensing in organs-on-chip using electroactive polymers. 2020.
- [24] Thanh Tung Nguyen, Vinh Khanh Nguyen, Youngtai Yoo, and Nam Seo Goo. A novel polymeric micropump based on a multilayered ionic polymer-metal composite. In *IECON Proceedings (Industrial Electronics Conference)*, pages 4888–4893, 2006. ISBN 1424401364. doi: 10.1109/IECON.2006.347352. URL <https://ieeexplore.ieee.org/ielx5/4152824/4152825/04153110.pdf?tp=&arnumber=4153110&isnumber=4152825&ref=aHR0cHM6Ly9pZWVleHBsb3JlLm1lZWUub3JnL2Fic3RyYWNOL2RvY3VtZW50LzQxNTMxMTA=>.
- [25] Vinh Khanh Nguyen, Jang Woo Lee, and Youngtai Yoo. Characteristics and performance of ionic polymer-metal composite actuators based on Nafion/layered silicate and Nafion/silica nanocomposites. *Sensors and Actuators, B: Chemical*, 120(2):529–537, 2007. ISSN 09254005. doi: 10.1016/j.snb.2006.03.015.

- [26] Attila Oláh, Henrik Hillborg, and G. Julius Vancso. Hydrophobic recovery of UV/ozone treated poly(dimethylsiloxane): Adhesion studies by contact mechanics and mechanism of surface modification. *Applied Surface Science*, 239(3-4):410–423, 1 2005. ISSN 01694332. doi: 10.1016/j.apsusc.2004.06.005. URL <https://www.sciencedirect.com/science/article/pii/S0169433204009444>.
- [27] Harry Olson, Graham Betton, Denise Robinson, Karluss Thomas, Alastair Monro, Gerald Kolaja, Patrick Lilly, James Sanders, Glenn Sipes, William Bracken, Michael Dorato, Koen Van Deun, Peter Smith, Bruce Berger, and Allen Heller. Concordance of the toxicity of pharmaceuticals in humans and in animals. *Regulatory Toxicology and Pharmacology*, 32(1):56–67, 2000. ISSN 02732300. doi: 10.1006/rtp.2000.1399.
- [28] Kyall Pocock, Ludivine Delon, Vaskor Bala, Shasha Rao, Craig Priest, Clive Prestidge, and Benjamin Thierry. Intestine-on-A-Chip Microfluidic Model for Efficient in Vitro Screening of Oral Chemotherapeutic Uptake. *ACS Biomaterials Science and Engineering*, 3(6):951–959, 2017. ISSN 23739878. doi: 10.1021/acsbiomaterials.7b00023. URL <https://pubs.acs.org/sharingguidelines>.
- [29] Joshi-Mukherjee R. Heart-on-a-Chip Model for Cardiomyopathies. *International Journal of Stem Cell Research and Transplantation*, pages 1–3, 2017. doi: 10.19070/2328-3548-1700011e. URL <http://scidoc.org/IJST.php>.
- [30] Bastian E. Rapp. *Microfluidics: Modelling, Mechanics and Mathematics*. 2017. doi: 10.1016/b978-1-4557-3141-1.50034-4.
- [31] Mario Rothbauer, Julie M Rosser, Helene Zirath, and Peter Ertl. Tomorrow today: organ-on-a-chip advances towards clinically relevant pharmaceutical and medical in vitro models, 2 2019. ISSN 18790429. URL <https://linkinghub.elsevier.com/retrieve/pii/S0958166918300570>.
- [32] S. Singh, N. Kumar, D. George, and A. K. Sen. Analytical modeling, simulations and experimental studies of a PZT actuated planar valveless PDMS micropump. *Sensors and Actuators, A: Physical*, 225:81–94, 2015. ISSN 09244247. doi: 10.1016/j.sna.2015.02.012.
- [33] Erik Stemme and Göran Stemme. A valveless diffuser/nozzle-based fluid pump. *Sensors and Actuators: A. Physical*, 39(2):159–167, 1993. ISSN 09244247. doi: 10.1016/0924-4247(93)80213-Z.
- [34] Michael W. Toepke and David J. Beebe. PDMS absorption of small molecules and consequences in microfluidic applications. *Lab on a Chip*, 6(12):1484, 11 2006. ISSN 1473-0197. doi: 10.1039/b612140c. URL <http://xlink.rsc.org/?DOI=b612140c>.
- [35] Amos Ullmann. The piezoelectric valve-less pump - Performance enhancement analysis. *Sensors and Actuators, A: Physical*, 69(1):97–105, 1998. ISSN 09244247. doi: 10.1016/S0924-4247(98)00058-2.
- [36] U.S. Food and Drug Administration. The drug development process | FDA, 2019. URL <https://www.fda.gov/patients/learn-about-drug-and->.
- [37] Marinke W. van der Helm, Andries D. van der Meer, Jan C.T. Eijkel, Albert van den Berg, and Loes I. Segerink. Microfluidic organ-on-chip technology for blood-brain barrier research. *Tissue Barriers*, 4(1), 2016. ISSN 21688370. doi: 10.1080/21688370.2016.1142493.
- [38] Paul M Van Midwoud, Geny M.M. Groothuis, Marjolijn T. Merema, and Elisabeth Verpoorte. Microfluidic biochip for the perfusion of precision-cut rat liver slices for metabolism and toxicology studies. *Biotechnology and Bioengineering*, 105(1):184–194, 1 2010. ISSN 00063592. doi: 10.1002/bit.22516. URL <http://doi.wiley.com/10.1002/bit.22516>.
- [39] Christophe Yamahata, C. Lotto, E. Al-Assaf, and M. A.M. Gijs. A PMMA valveless micropump using electromagnetic actuation. *Microfluidics and Nanofluidics*, 1(3):197–207, 2005. ISSN 16134982. doi: 10.1007/s10404-004-0007-6.
- [40] Yu Zhou and Farid Amirouche. An electromagnetically-actuated all-pdms valveless micropump for drug delivery. *Micromachines*, 2(3):345–355, 2011. ISSN 2072666X. doi: 10.3390/mi2030345.

Appendices



Beam theory

Although the movement of a membrane is well defined, for this study other mechanics are used. This was a conscious choice: the available data for the behavior of this specific material was based on a test with a cantilever beam [23]. This can not simply be translated to the behaviour of a membrane of the same material: the driving force might act differently. In order to provide data based on well defined assumptions rather than disregarding numerous possible side-effects, the beam-approach described below is used.

The IPMC to be used has been tested in a cantilever beam setup [23] from which some characteristics can be determined. In figure A.1 a qualitative sketch of the situation is given. Note that the beam is assumed to be clamped at the origin.

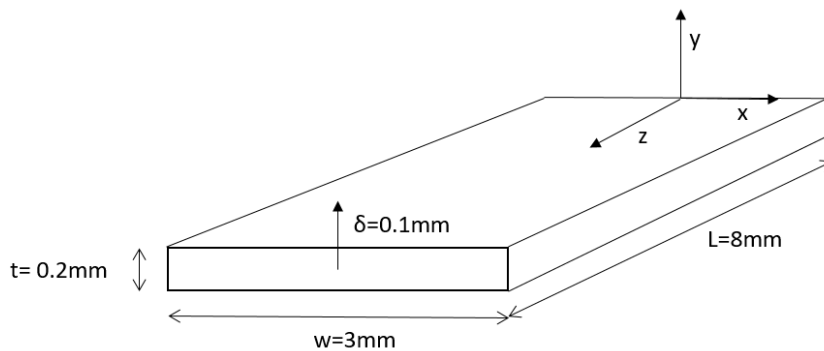


Figure A.1: Qualitative sketch of the IPMC cantilever beam. It is clamped at the origin.

The vertical displacement v of a cantilever beam with symmetric cross-section relates to the flexural rigidity through the following equation [22]:

$$\frac{d^2 v}{dz^2} = -\frac{M_x(z)}{EI_{xx}}$$

With M_x the moment about the x-axis, E the Youngs modulus, I_{xx} the second moment of area about the x-axis, and v the vertical displacement (in y-direction). The tip displacement $v(L)$ is δ (see figure A.1). The experimental data showed a Youngs modulus of $E = 650\text{MPa}$. Furthermore, for a cantilever beam with a clamped origin, the moment along the beam can be described as:

$$M_x = P(L - z) \quad \text{or} \quad M_x = qx(L - z)$$

with P a shear force or q the distributed load. For convenience a tip load P is assumed for this case.

In order to find the equation for deflection the moment equation above is integrated twice:

$$\begin{aligned}
 v &= \iint -\frac{M_x(z)}{EI_{xx}} \\
 &= -\frac{P}{EI_{xx}} \iint (L-z) \\
 &= -\frac{P}{EI_{xx}} \left(L\frac{z^2}{2} - \frac{z^3}{6} \right) + C_1z + C_2 \\
 &= -\frac{Pz^2}{2EI_{xx}} \left(L - \frac{z}{3} \right) + C_1z + C_2
 \end{aligned}$$

The integration constants are determined by applying the boundary conditions for this case. For a clamped beam, $v(0) = 0$ and $\theta(0) = v'(0) = 0$ (by definition). This yields:

$$v = -\frac{Pz^2}{2EI_{xx}} \left(L - \frac{z}{3} \right)$$

The unknown is P , so for $z = L$ and $v(L) = \delta$:

$$P = \delta \frac{3EI_{xx}}{L^3}$$

The second moment of area about the x-axis of this beam is:

$$I_{xx} = \frac{w \left(\frac{t}{2} \right)^3}{12} = \frac{wt^3}{96}$$

And so:

$$\begin{aligned}
 P &= \delta \frac{3Ewt^3}{96L^3} \\
 &= 0.1 \frac{650 \cdot 3 \cdot 0.2^3}{32 \cdot 8^3} \\
 &= 9.52 \cdot 10^{-5} \text{ N}
 \end{aligned}$$

This is the shear force induced by the applied voltage, yielding a maximum deflection of 0.1 mm for a clamped beam. If now the two possible variables are now taken to be the membrane displacement and the membrane size, the relation becomes:

$$\begin{aligned}
 \delta &= \frac{PL^3}{3EI_{xx}} \\
 &= \frac{96 \cdot 9.52 \cdot 10^{-5} \cdot L^3}{3 \cdot 650 \cdot 3 \cdot 0.2^3} \\
 &= 1.95 \cdot 10^{-4} \cdot L^3 \text{ [mm]}
 \end{aligned}$$

However, the conditions in the pump are somewhat different. Not only is there true free-moving tip, the membrane size differs and the behaviour of a membrane overall differs from that of a cantilever. Moreover, this is a frame that can be set for the available test data, which is preferred over possibly unreliable theoretical assumptions.

Unless mentioned otherwise, the following assumptions apply:

- The moving membrane consists of a PDMS sealing sheet with one actuating cantilever IPMC beam attached to the fluid side.
- The stiffness of the IPMC cantilever is much higher than the stiffness of the PDMS sealing sheet. (A conscious choice can be made here for a soft PDMS mixture.)
- the thickness of the PDMS sheet does not contribute to the behavior of the cantilever significantly (as a result of this lower stiffness).

With this in mind the above relation can be used as an upper bound for the membrane displacement.

B

Supplementary plots

B.1. Frequency sweep

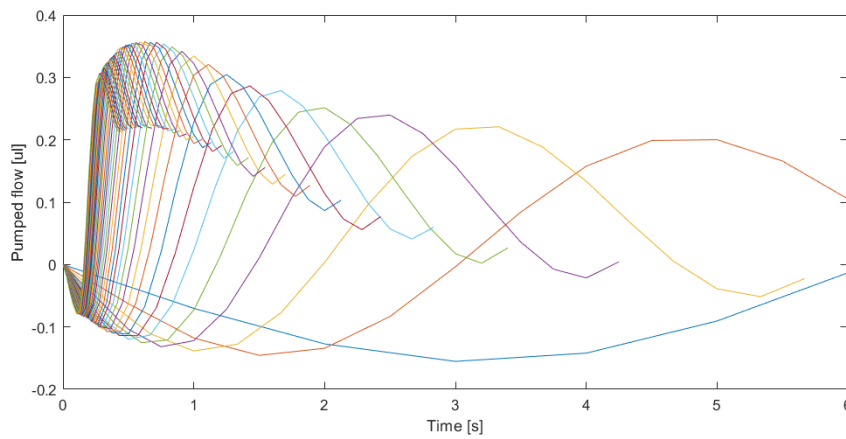


Figure B.1: Pumped flow development for varying frequency. Note that to display a legend would be impractical here: the frequency goes from 0.5Hz (longest period) to 20Hz (shortest period). The latter time segment is not displayed to show more detail in the first part.

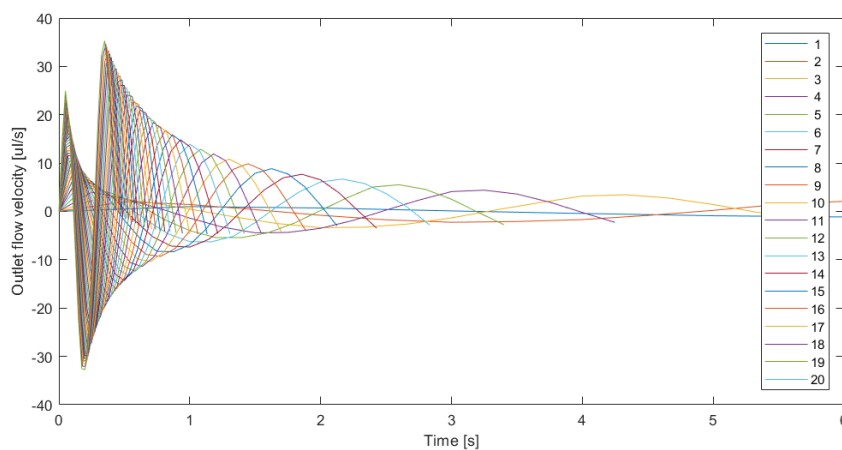


Figure B.2: Outflow as a function of time. Note that to display a legend would be impractical here: the frequency goes from 0.5Hz (longest period) to 20Hz (shortest period). The latter time segment is not displayed to show more detail in the first part.

B.2. Channel depth sweep

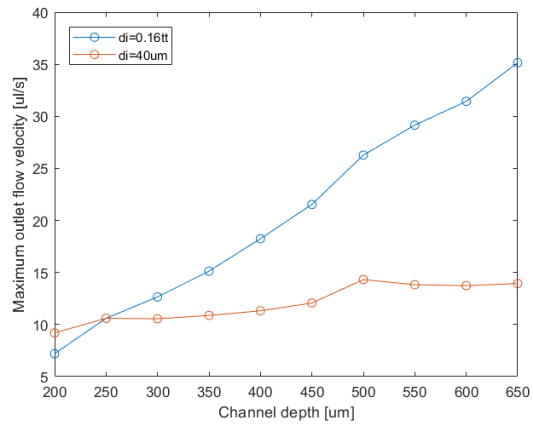
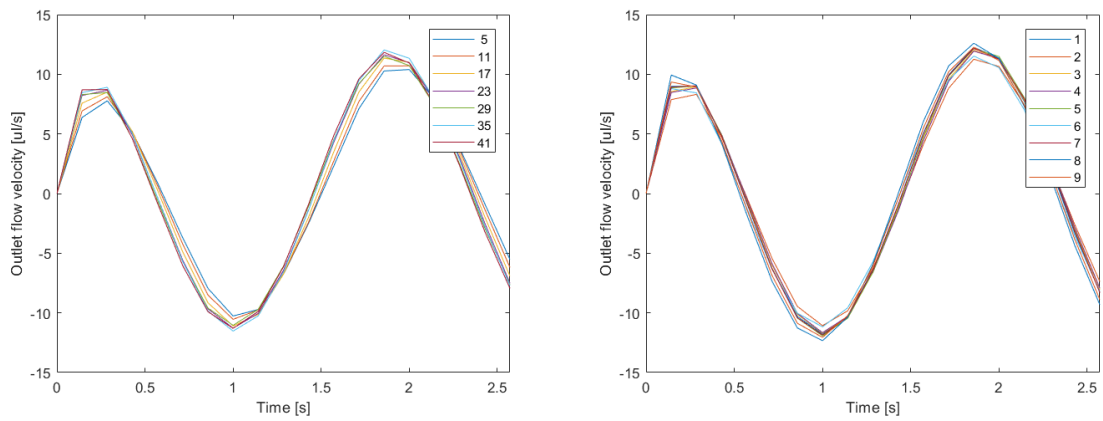


Figure B.3: The maximum outlet flow as a function of channel depth for constant relative and absolute membrane displacement.

B.3. Nozzle parameter sweeps



(a) The maximum outlet flow as a function of nozzle angle (b) The maximum outlet flow as a function of nozzle length

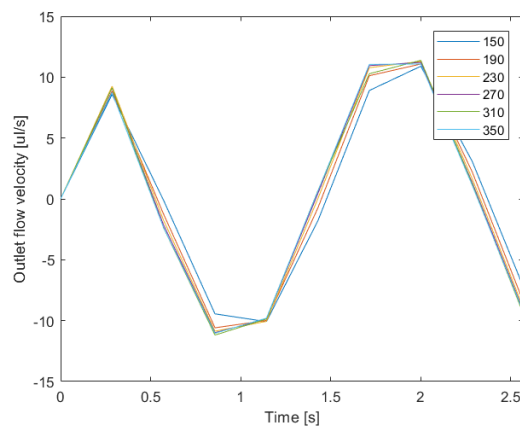
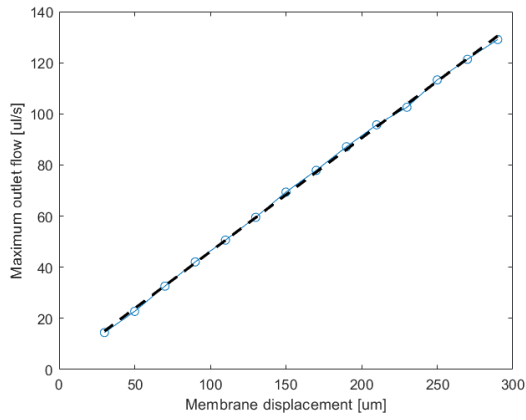
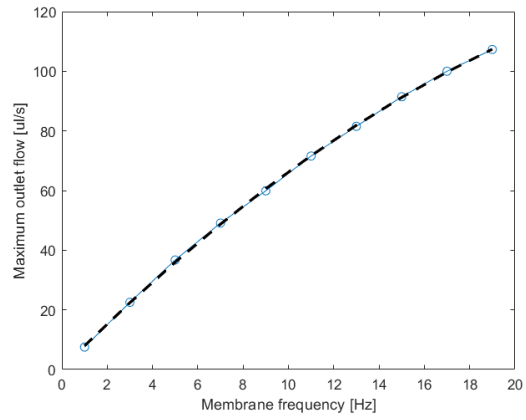


Figure B.5: The maximum outlet flow as a function of nozzle throat width

B.4. High flow rate design



(a) Varying membrane displacement ($f=3.5\text{Hz}$)



(b) Varying membrane frequency ($d_i=56\mu\text{m}$)

Figure B.6: Maximum outlet flow for the 'high flow rate' design

C

Matlab scripts

In this appendix a number of relevant MATLAB scripts are printed to give the reader more insight in the data processing. It must be noted that these scripts were not copied directly: some administrative lines were removed to improve readability for this report.

C.1. Sample time analysis

```
1 % A script to determine the time where the extrapolated flow rate of a
2 % dataset converges to the flowrate-per-minute value
3
4 imp    =   importdata('filename.txt');           % Data import
5 data   =   imp.data;                             % Separate data points
6 header =   imp.textdata;                         % Separate column headers
7
8 % Identify columns
9 t=data(:,1);                                     % Time column
10 dd=data(:,2:size(data,2));                      % Data matrix
11
12 % Take the first segment and calculate the fitted curve and the associated flowrate:
13 dstep  =   1;
14 ttot   =   length(t);
15
16 for i=1:(ttot-1)/dstep
17     ttemp =   t(1:dstep*i);
18     ddtemp =   dd(1:dstep*i);
19     fit(i,:) =   polyfit(ttemp,ddtemp,1);
20 end
21
22 flow    =   fit(:,1)*60+fit(2);
23
24 % Determine the ratios of flow and flow(end)
25 for i=1:length(flow)
26     flowrat(i) =   flow(i)/flow(end);
27 end
28
29 % Draw a dash line for y=1
30 ttemp   =   1:dstep:ttot-1;
31 one     =   ones(1,size(ttemp,2));
32
33 % Plot it
34 plot(ttemp,flowrat,'*')
35 xlabel('Number of datapoints [-]')
36 ylabel('Accuracy ratio')
37 hold on
38 plot(ttemp,one,'--k');
39 xlim([0,max(ttemp)+1]);
```

C.2. Single parameter sweep analysis

```

1 %% This script processes a single parameter sweep
2
3 vpump      =      importdata('disweep-vpump.txt');
4 Uout       =      importdata('disweep-Uout.txt');
5 vvdata     =      importdata('disweep-v.txt');
6
7 % What data is processed?
8 var        =      'Membrane displacement [um]';
9
10 % Other global variables
11 m          =      18;           % Sample time: datapoints+1, since 0 is included too
12 linvar     =      40;           % The parameter value from which the flow rate ...
    develops linearly
13 polydeg   =      1;           % The polynomial degree (enter zero if there is no ...
    trendline)
14 xcorr     =      1;           % if a unit correction is needed, otherwise put 1
15                                     % (for example when x is in rad instead of deg)
16
17 %% Flow rate
18
19 imp        =      vpump;
20 [xvector,tarray,dd] =      impprocess(imp,m);
21 %%
22 figure(1)
23 plot(tarray,dd)
24 xlabel('Time [s]')
25 ylabel('Pumped volume [ul]')
26 xlim([0 tarray(end,1)])
27 legend(num2str(xvector(1:2:end)))
28
29 flow       =      flowratefun(dd,tarray);
30 xvector    =      xcorr*xvector;
31
32 figure(2)
33 plot(xvector,flow,'-o')
34 xlabel(var)
35 ylabel('Flow rate [ul/min]')
36 hold on
37
38 lin        =      find(xvector==linvar*xcorr);
39 if polydeg==1
40     flowfit =      linearfit(flow,xvector,lin);
41 elseif polydeg==2
42     flowfit =      quadfit(flow,xvector,lin);
43 end
44
45 %% Uout
46 imp        =      Uout;
47 [xvector,tarray,dd] =      impprocess(imp,m);
48
49 xvector    =      xcorr*xvector;
50
51 figure(3)
52 plot(tarray,dd)
53 xlabel('Time [s]')
54 ylabel('Outlet flow velocity [ul/s]')
55 xlim([0 tarray(end,1)])
56 legend(num2str(xvector(2:2:end)))
57
58 for i=1:length(xvector)
59     Umax(i) =      max(dd(:,i));
60 end
61
62 figure(4)
63 plot(xvector,Umax,'-o')
64 xlabel(var)
65 ylabel('Maximum outlet flow velocity [ul/s]')

```

```
66
67 %% Vprofile
68 if exist('vvddata')==1           % Skip it if there is no vvddata file
69 imp = vvddata;
70 [xvector,tarray,dd] = impprocess(imp);
71
72 vmax = max(dd);
73
74 figure(6)
75 plot(xvector,vmax,'-o')
76 xlabel(var)
77 ylabel('Maximum center line flow velocity [mm/s]')
78 hold on
79
80 fit = polyfit(xvector',vmax,2);
81 fitfit = fit(1)*xvector.^2+fit(2)*xvector+fit(3);
82 plot(xvector,fitfit,'--k','Linewidth',2)
83 end
```

C.3. Flowrate calculation

```
1 function [flow] = flowratefun(dd,tarray)
2 % This function calculates the flowrate based on vpump data
3
4 for i=1:size(dd,2)
5     if size(tarray,2)==1 % Distinguishes between a constant time vector or varying
6         flowfit(i,:)=polyfit(tarray,dd(:,i),1);
7     else
8         flowfit(i,:)=polyfit(tarray(:,i),dd(:,i),1);
9     end
10 end
11
12 flow=60*flowfit(:,1)+flowfit(:,2); % Flow rate in ul/min
13
14 end
```


D

Model sketches

Below the pump setups have been sketched in a possible setup. On the top side the pump chamber is depicted along with the nozzle-diffuser elements. To minimize flow changes outside the pump environment the width of the channel is constant throughout the cycle. On the lower side, a chamber is placed to simulate a test well where for example cells are cultured: however, the chamber might just as well be continuous, this is merely a setup proposal.

Note also that the models are scaled with respect to one another.

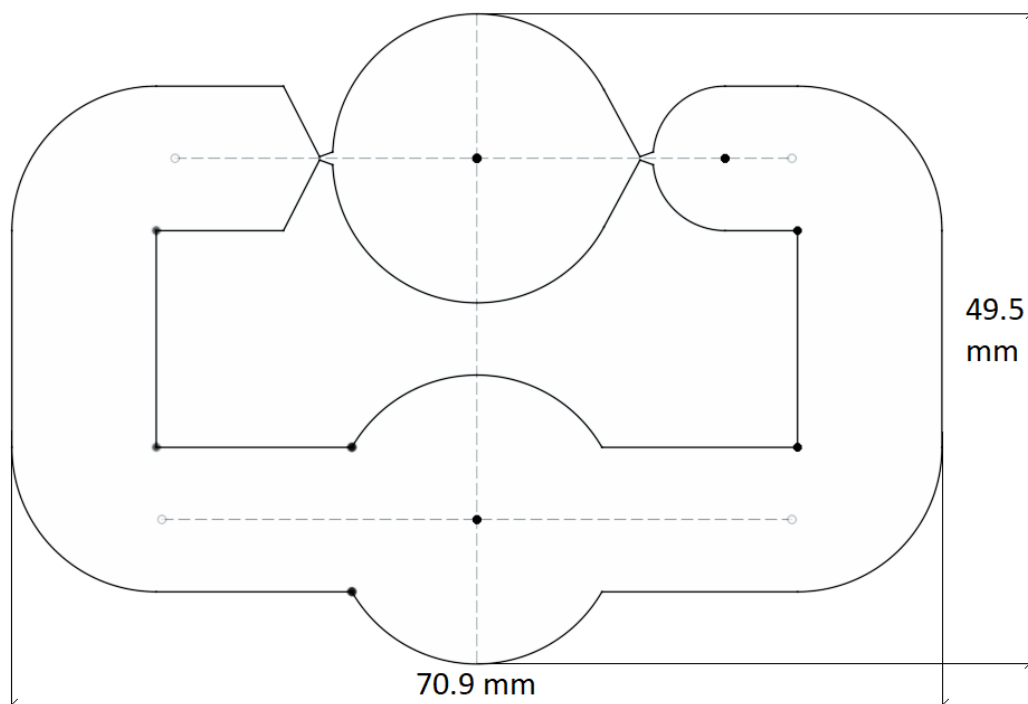


Figure D.1: "High flow rate" model test setup

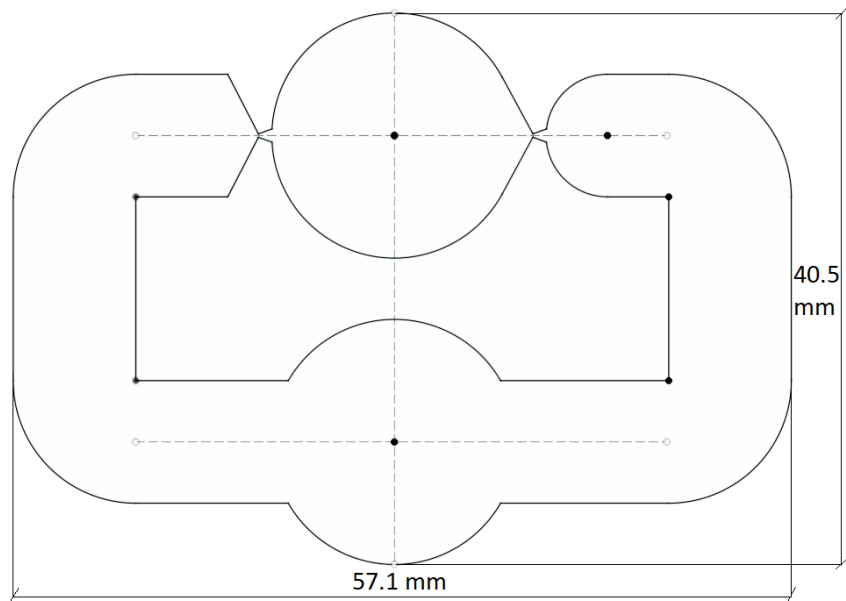


Figure D.2: "High flow pulse" model test setup

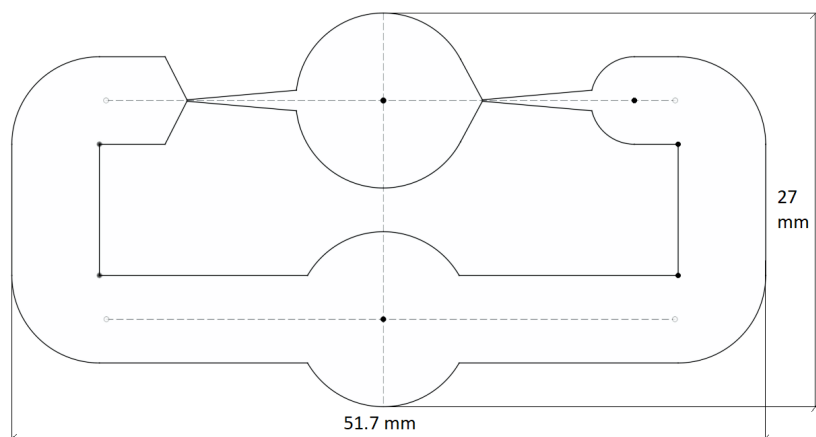


Figure D.3: "Low flow rate and pulse" model test setup

Acronyms

BBB	blood-brain barrier
DAE	differential algebraic equation
EKL	Else Kooi Laboratory
IND	investigational new drug
IPMC	ionic polymer-metal composite
MEMS	micro-electronical mechanical systems
NCE	new chemical entity
ODE	ordinary differential equation
OoC	organ-on-chip
PDMS	polydimethylsiloxane
PMMA	polymethylmethacrylate

Glossary

in vitro

Latin for 'in glass' or the study of cells or microorganisms outside of their normal environment. 5

in vivo

Latin for 'within the living' or the study of certain processes in living organisms or cells. v, 3, 4, 8, 9

alveoli

Cells of the lung tissue allowing the exchange of gases from the blood to the air in the lungs. 6

angiogenesis description

. 4

astrocyte

Nervous cells in the brain and spinal cord, directing the blood-brain barrier and providing the nervous tissue with nutrients. 4

atherosclerosis

Formation of small thickening fatty patches in the vessel lumen, blocking blood flow and stiffening the wall. 5, 13

blood-brain barrier

A protective layered mechanism that helps maintain the brain's stable environment. 4-6

cardiac potential

Spontaneous change in membrane potential in cardiac muscle cells, triggering rhythmic contractions. 4, 8

hepatocyte

Liver cells capable of producing bile, process bloodborne nutrients, store fat-soluble vitamins and rid the blood of certain toxins. 4

microbiome

The culture of microorganisms that exists, for example, in the intestine. 4, 7

microvilli

cellular membrane extensions with the function of drastically increasing the absorptive area (in the intestine). 4, 5

nephron

Functional unit of the kidney, filtering blood and producing urine. 4

pathology

Disease and/or injury and their study. 4, 5

physiology

The study of the function of organisms, or how they carry out life-sustaining activities. 1, 3, 4

shear

The component of force or stress in-plane with the material it is acting on. 3–6, 8–10, 13

surfactant

Liquid which lowers the surface tension, for example present in the alveolar cells. 4, 7